Article

SLC25A51 is a mammalian mitochondrial NAD$^+$ transporter

https://doi.org/10.1038/s41586-020-2741-7

Received: 22 December 2019

Accepted: 1 September 2020

Published online: 9 September 2020

Check for updates

Timothy S. Luongo[1], Jared M. Eller[2], Mu-Jie Lu[2], Marc Niere[3], Fabio Raith[4,5], Caroline Perry[1], Marc R. Bornstein[1], Paul Oliphint[2], Lin Wang[6], Melanie R. McReynolds[6], Marie E. Migaud[7], Joshua D. Rabinowitz[6], F. Brad Johnson[8], Kai Johnsson[4,9], Mathias Ziegler[3], Xiaolu A. Cambronne[2]✉ & Joseph A. Baur[1]✉

Mitochondria require nicotinamide adenine dinucleotide (NAD$^+$) to carry out the fundamental processes that fuel respiration and mediate cellular energy transduction. Mitochondrial NAD$^+$ transporters have been identified in yeast and plants[1,2], but their existence in mammals remains controversial[3–5]. Here we demonstrate that mammalian mitochondria can take up intact NAD$^+$, and identify SLC25A51 (also known as MCART1)—an essential[6,7] mitochondrial protein of previously unknown function—as a mammalian mitochondrial NAD$^+$ transporter. Loss of SLC25A51 decreases mitochondrial—but not whole-cell—NAD$^+$ content, impairs mitochondrial respiration, and blocks the uptake of NAD$^+$ into isolated mitochondria. Conversely, overexpression of SLC25A51 or SLC25A52 (a nearly identical paralogue of SLC25A51) increases mitochondrial NAD$^+$ levels and restores NAD$^+$ uptake into yeast mitochondria lacking endogenous NAD$^+$ transporters. Together, these findings identify SLC25A51 as a mammalian transporter capable of importing NAD$^+$ into mitochondria.

NAD$^+$ is a vital cofactor for the metabolic reactions that fuel life. NAD$^+$ functions as an electron acceptor (through hydride transfer) for hundreds of reactions, becoming reduced to NADH in the process. NADH subsequently provides reducing power throughout the cell, including to complex I of the mitochondrial electron transport chain to drive cellular respiration. Owing to the requirement for NAD$^+$ in both glycolysis and mitochondrial respiration, cells possess no sustainable means to produce ATP in the absence of NAD$^+$. In addition to its redox roles, NAD$^+$ is also a substrate for multiple classes of signalling enzymes including sirtuins, ADP-ribosyltransferases and cyclic ADP-ribose synthases[8]. Thus, changes in NAD$^+$ availability can influence cellular behaviour even at concentrations that do not interfere directly with metabolism, whereas a complete lack of NAD$^+$ is lethal.

Despite more than 100 years of research[3] on NAD$^+$, and intense focus on NAD$^+$-dependent processes within the mitochondrial matrix, the question of how mammalian mitochondria obtain their NAD$^+$ pool has never been answered. The mitochondrial NAD$^+$ pool is distinct from the cytosolic pool[4,9,10], and may be regulated independently under stress[11]. Yeast and plants possess well-characterized transporters embedded in the inner mitochondrial membrane[1,2]. However, no obvious homologues exist in mammals, and the most closely related transporter has been characterized as a mitochondrial carrier for folate[12] and flavin adenine dinucleotide[13]. On the basis of the existence of a mitochondrial nicotinamide mononucleotide adenylyltransferase (NMNAT3), it has been suggested[14] that mitochondria might take up cytosolic nicotinamide mononucleotide and subsequently convert it to NAD$^+$. A minority of nicotinamide phosphoribosyltransferase (NAMPT) also co-purifies with liver mitochondria, leading to the alternative suggestion that mitochondria might possess an intact pathway to synthesize NAD$^+$ directly from nicotinamide[4]. However, mitochondria from several mammalian cell types lack active NAMPT, arguing against this as a universal mechanism[10,15–17]. In addition, mice lacking NMNAT3 survive to adulthood and exhibit no overt change in mitochondrial NAD$^+$ content[18,19]. It was recently shown that isolated mitochondria do not synthesize NAD$^+$ within the matrix from exogenous nicotinamide or nicotinamide mononucleotide (NMN), but that stable-isotope labelled NAD$^+$ can be taken up from the cytosol[15]. Thus, data support the existence of a mammalian mitochondrial NAD$^+$ transporter, but its molecular identity has remained unknown.

Here we identify SLC25A51 as a mammalian mitochondrial NAD$^+$ transporter. We considered SLC25A51 as a candidate because the corresponding gene was identified as essential in several genome-wide screens[6,7], and it is a member of the mitochondrial carrier family that has not previously been assigned a function (Extended Data Table 1). We show that expression of SLC25A51 dictates mitochondrial NAD$^+$ levels and uptake capacity in mammalian cells and complements yeast lacking their known mitochondrial NAD$^+$ transporters. A nearly identical paralogue, SLC25A52, is also capable of restoring NAD$^+$ uptake in yeast, but is not widely expressed[20]. Thus, SLC25A51-dependent direct

[1]Department of Physiology and Institute for Diabetes, Obesity, and Metabolism, Perelman School of Medicine, University of Pennsylvania, Philadelphia, PA, USA. [2]Department of Molecular Biosciences, University of Texas at Austin, Austin, TX, USA. [3]Department of Biomedicine, University of Bergen, Bergen, Norway. [4]Department of Chemical Biology, Max Planck Institute for Medical Research, Heidelberg, Germany. [5]Faculty of Chemistry and Earth Sciences, University of Heidelberg, Heidelberg, Germany. [6]Lewis-Sigler Institute for Integrative Genomics, Department of Chemistry, Princeton University, Princeton, NJ, USA. [7]Mitchell Cancer Institute, University of South Alabama, Mobile, AL, USA. [8]Department of Pathology and Laboratory Medicine, Perlman School of Medicine, University of Pennsylvania, Philadelphia, PA, USA. [9]Institute of Chemical Sciences and Engineering, École Polytechnique Fédérale de Lausanne (EPFL), Lausanne, Switzerland. ✉e-mail: lulu@austin.utexas.edu; baur@pennmedicine.upenn.edu

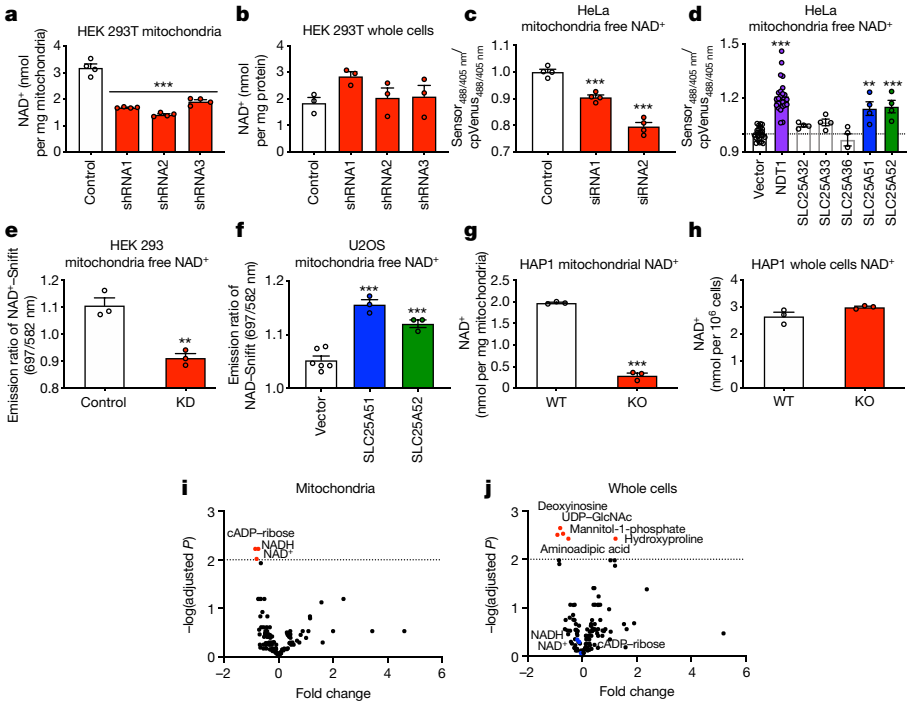

Fig. 1 | SLC25A51 and SLC25A52 expression dictates mitochondrial NAD$^+$ concentration. a, **b**, NAD$^+$ content of isolated mitochondria ($n = 4$) (**a**) and whole-cell lysates ($n = 3$) (**b**) from HEK 293T cells stably depleted of *SLC25A51* (shRNA1–3) and stably expressing non-targeting control shRNA (control). **c**, Mitochondrial free NAD$^+$ levels in HeLa cells transfected with siRNA targeting *SLC25A51* (siRNA1 and siRNA2) and non-targeting siRNA (control), measured by the mitochondrially-targeted cpVenus NAD$^+$ biosensor, ($n = 4$). **d**, Mitochondrial free NAD$^+$ levels in HeLa cells overexpressing NDT1 (yeast mitochondrial NAD$^+$ transporter) ($n = 24$), SLC25A32 ($n = 4$), SLC25A33 ($n = 4$), SLC25A36 ($n = 4$), SLC25A51 ($n = 4$), SLC25A52 ($n = 4$) or vector control ($n = 24$), measured by the cpVenus NAD$^+$ biosensor. **e**, Mitochondrial free NAD$^+$ levels in HEK 293 cells with stable shRNA-mediated knockdown of *SLC25A51* ($n = 3$) and stable expression of non-targeting shRNA (control) ($n = 3$). **f**, Mitochondrial free NAD$^+$ levels in U2OS cells overexpressing SLC25A51, SLC25A52 and vector control ($n = 6$), as measured by NAD$^+$–Snifit. **g**, **h**, Mitochondrial ($n = 3$) (**g**) and whole-cell NAD$^+$ content ($n = 3$) (**h**) of lysates collected from CRISPR–Cas9-mediated SLC25A51-KO and wild-type (WT) HAP1 cells. **i**, **j**, Mitochondrial ($n = 3$) (**i**) and whole-cell ($n = 3$) (**j**) metabolomes of HAP1 SLC25A51-KO and wild-type cells measured by liquid chromatography–mass spectrometry. Significantly changed metabolites were determined by setting a false discovery rate of 1% (two-stage step-up method of Benjamini, Krieger and Yekutieli) and are represented in a volcano plot. *n* represents biologically independent replicates. Data are mean ± s.e.m. *P* values were determined by unpaired, two-tailed Student's *t*-test (for two groups) or one-way analysis of variance (ANOVA) with multiple comparisons analysis using Dunnett's method (for groups of three or more). $^{**}P < 0.01$, $^{***}P < 0.001$ versus control, vector or wild type (exact *P* values are provided in the Source Data).

uptake is an important mechanism by which mammalian mitochondria obtain NAD$^+$.

SLC25A51 sets mitochondrial NAD$^+$ levels

To test whether SLC25A51 has a role in mitochondrial NAD$^+$ homeostasis, we performed knockdown experiments in human cell lines using multiple distinct short hairpin (sh)RNA and small interfering (si)RNA sequences. We found that SLC25A51 is required for the maintenance of mitochondrial NAD$^+$ levels (Fig. 1a, Extended Data Fig. 1a–c) but does not affect total cellular NAD$^+$ content (Fig. 1b, Extended Data Fig. 1d). To measure mitochondrial free NAD$^+$ concentrations in intact cells and avoid any artefacts that might be produced during isolation, we next used two distinct mitochondrially targeted NAD$^+$ biosensors. The first sensor couples an engineered NAD$^+$-binding domain with circularly permutated Venus (cpVenus) to report local concentrations of free NAD$^+$ via ratiometric changes in the fluorescence intensity[9]. This method confirmed a decline in mitochondrial free NAD$^+$ levels in SLC25A51-deficient tumour cells and mouse embryonic stem cells (Fig. 1c, Extended Data Fig. 1e–g). Overexpression of either SLC25A51 or SLC25A52 was sufficient to increase mitochondrial free NAD$^+$ levels, similar to the effect of overexpressing the yeast mitochondrial NAD$^+$ transporter NDT1, whereas candidates with greater homology to NDT1 had no effect (Fig. 1d, Extended Data Fig. 1h). The effects of SLC25A51 and SLC25A52 on mitochondrial free NAD$^+$ levels were confirmed using the fluorescence resonance energy transfer (FRET)-based NAD$^+$–Snifit biosensor[21] (Fig. 1e, f). Both Flag–haemagglutinin (HA)–SLC25A51 and Flag–HA–SLC25A52 co-localized with the mitochondrial marker MTC02 (Extended Data Fig. 1i). We focused primarily on SLC25A51 rather than SLC25A52 because SLC25A52 exhibits a more restricted expression pattern[20] and has not emerged as essential in screens performed to date[6,7,22,23].

To understand the consequences of total SLC25A51 loss, we studied SLC25A51-knockout (KO) HAP1 cells generated using CRISPR–Cas9, in which SLC25A51 was previously reported to be non-essential[22]. Targeted cells survived and proliferated, albeit at a reduced rate, similar to cell lines with shRNA-based knockdowns (Extended Data Fig. 1j–l). No compensatory upregulation of SLC25A52 was detected in any of the cell lines (Extended Data Fig. 1m–o), although its expression may have contributed to the survival of SLC25A51-KO cells and may account for a residual band that was apparent when blotting for SLC25A51 protein (Extended Data Fig. 1p). SLC25A51-KO cells exhibited loss of mitochondrial NAD$^+$ (Fig. 1g), but not of total cellular NAD$^+$ (Fig. 1h). Metabolomic profiling revealed that only NAD$^+$, NADH and the NAD$^+$-derived metabolite cyclic ADP-ribose were significantly changed in mitochondrial extracts of SLC25A51-KO cells (Fig. 1i, Extended data Fig. 1q). By contrast, NAD$^+$ and NADH levels were unchanged in whole-cell extracts of SLC25A51-KO cells, whereas several sugars and nucleotide-related metabolites were

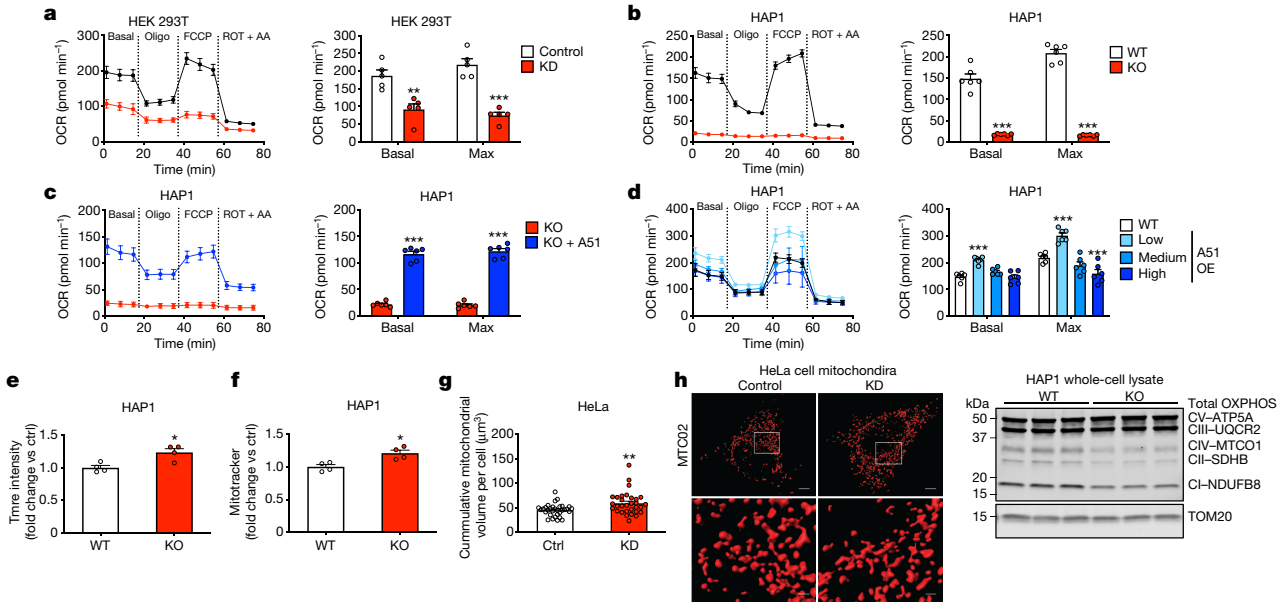

Fig. 2 | SLC25A51 modulates mitochondrial respiratory capacity. **a**–**d**, Oxygen consumption rate (OCR) for SLC25A51 shRNA-depleted HEK 293T cells ($n = 5$) (**a**), HAP1 SLC25A51-KO cells ($n = 6$) (**b**), HAP1 SLC25A51-KO cells rescued using adenovirus-mediated SLC25A51 expression (multiplicity of infection (MOI) of 4) ($n = 6$) (**c**) and HAP1 wild-type cells with low (MOI = 2), medium (MOI = 4) and high (MOI = 6) overexpression (OE) of SLC25A51 ($n = 6$) (80,000 cells per well) (**d**). Basal OCR was measured before the addition of treatments and maximal respiration was measured after the sequential addition of the ATP synthase inhibitor oligomycin (oligo) and the oxidative phosphorylation uncoupler FCCP (uncoupler). Rotenone (Rot) and antimycin A (AA) were then added as a control to completely block mitochondrial oxygen consumption. **e**, Quantification of mitochondrial membrane potential using the cell-permeant fluorescent dye TMRE ($n = 4$). **f**, Mitochondrial content measured by fluorescence intensity of the mitochondrial localization dye, MitoTracker Deep Red ($n = 4$). Relative fluorescence intensities were determined by flow cytometry. **g**, Cumulative mitochondrial volume per cell quantified from confocal image reconstructions of mitochondrial voxels in *SLC25A51* shRNA knockdown ($n = 31$ cells) and control ($n = 32$ cells) HeLa cells. **h**, Representative images of mitochondrial voxels (mitochondrial marker, anti-MTC02) reconstructed using 0.1-µm optical slices and Imaris surface analyses. Scale bars, 5 µm (top), 1 µm (bottom). **i**, Western blot of mitochondrial oxidative phosphorylation complexes I–V (CI–CV) in SLC25A51-KO HAP1 cells. TOM20 was blotted as a mitochondrial-loading control. *n* represents biologically independent replicates unless otherwise indicated. Data are mean ± s.e.m. *P* values were determined by unpaired, two-tailed Student's *t*-test or two-way ANOVA with multiple comparisons analysis using Dunnett's method (for groups of three or more). $^{*}P < 0.05$, $^{**}P < 0.01$ and $^{***}P < 0.001$ versus control, wild type or SLC25A51-KO (exact *P* values are provided in the Source Data).

decreased and hydroxyproline was increased, probably reflecting a combination of impaired mitochondrial metabolism and increased reliance on glycolytic energy production (Fig. 1j, Extended Data Fig. 1r). Thus, loss of SLC25A51 results in selective loss of NAD^+ from the mitochondrial fraction.

Loss of SLC25A51 impairs mitochondria

Mitochondrial NAD^+ is essential for the tricarboxylic acid cycle to fuel oxidative phosphorylation. Loss of NAMPT activity causes NAD^+ deficiency and impairs mitochondrial respiration in mammalian cells and tissues[24,25]. Exogenous NAD^+ was sufficient to rescue respiratory capacity in mitochondria isolated from cells treated with the NAMPT inhibitor FK866 (Extended Data Fig. 2a), similar to a previous report using mitochondria isolated from cells cultured under nutrient-poor conditions[26]. SLC25A51 deficiency (Fig. 2a, Extended Data Fig. 2b,c) or knockout (Fig. 2b) impaired basal and maximal respiratory capacity in cells and complex I-dependent respiration in isolated mitochondria. However, exogenous NAD^+ was insufficient to restore respiration in mitochondria from cells with SLC25A51 knockdown (Extended Data Fig. 2d). Adenoviral expression of SLC25A51 restored respiration in SLC25A51-KO cells, and further increased the respiration of wild-type cells when added at a low, but not at a high, multiplicity of infection (Fig. 2d). This is consistent with previous observations that excess NDT1 or NDT2 activity decreases mitochondrial efficiency in yeast[27] and impairs respiration in mammalian cells[5]. Thus, expression of SLC25A51 markedly affects cellular respiration.

In contrast to respiratory capacity, mitochondrial membrane potential was maintained after SLC25A51 loss. Staining with tetramethylrhodamine ethylester (TMRE), which accumulates in mitochondria proportionally to their membrane potential, was modestly increased in SLC25A51-KO cells (Fig. 2e). This probably reflects an increase in mitochondrial abundance, rather than membrane potential, as a similar increase in signal was noted for cells stained with MitoTracker dye (Fig. 2f). A modest increase in mitochondrial volume was confirmed by staining mitochondria with MTC02 antibody in cells with shRNA-mediated depletion of *SLC25A51* and performing 3D reconstructions (Fig. 2g, h, Extended Data Fig. 2e, f). SLC25A51 is reported to interact with C7orf55, an assembly factor for complex V of the electron transport chain, and BOLA1, a protein that forms an iron–sulfur linked complex with glutaredoxin 5 and may be involved in oxidative stress resistance[28]. We detected no apparent change in the expression of the complex V subunit ATP5A (Fig. 2i) and note that uncoupling (bypassing complex V) did not restore respiration in SLC25A51-deficient cells (Fig. 2a, b, Extended Data Fig. 2b). However, expression of subunits of complexes I, II and IV were reduced (Fig. 2i), and we cannot rule out a contribution of changes in iron–sulfur cluster metabolism or oxidative stress to the observed effects of SLC25A51 deficiency.

SLC25A51 drives mitochondrial NAD^+ uptake

To test whether SLC25A51 mediates uptake of NAD^+ into mammalian mitochondria, we isolated organelles from SLC25A51-depleted and SLC25A51-KO cells and incubated them with exogenous NAD^+.

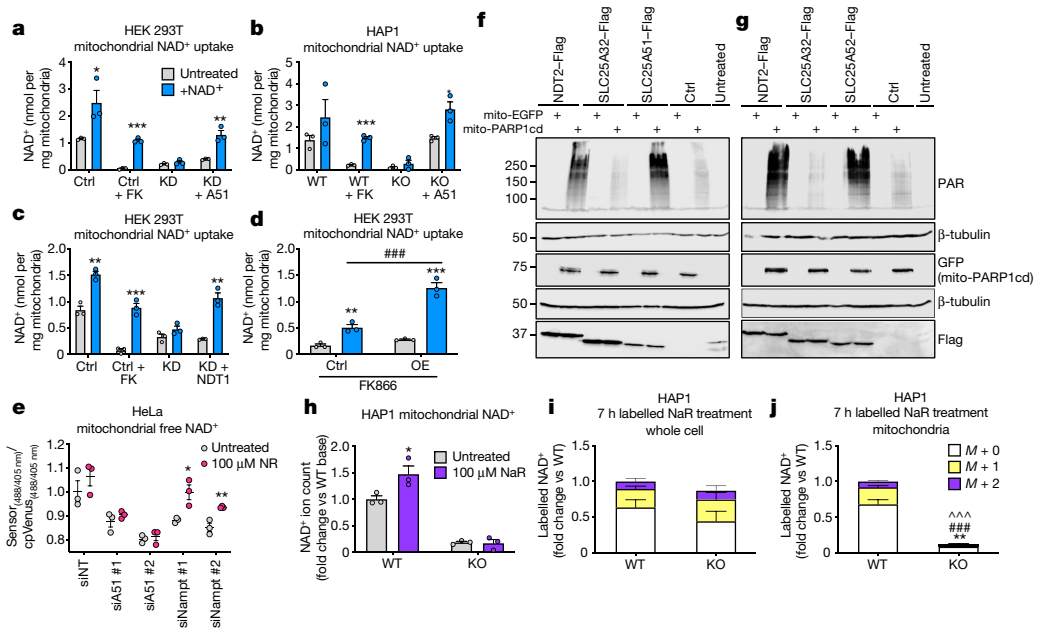

Fig. 3 | SLC25A51 expression is required for NAD$^+$ uptake in isolated mitochondria. a, NAD$^+$ content of isolated mitochondria measured before and after a 40-min incubation with 1 mM NAD$^+$ from HEK 293T control (ctrl) cells, control cells treated with FK866 (ctrl + FK) to deplete mitochondrial NAD$^+$, *SLC25A51* shRNA-knockdown (KD) cells, and cells with *SLC25A51*-KD transfected with mouse *Slc25a51* cDNA (KD + A51). **b**, As **a**, but for wild-type HAP1 cells, HAP1 cells treated with FK866 (WT + FK), SLC25A51-KO cells, and SLC25A51-KO cells transduced with adenovirus encoding SLC25A51 (KO + A51). **c**, As **a**, but for HEK 293T control (ctrl) cells, control cells treated with FK866 (ctrl + FK), *SLC25A51*-KD cells, and *SLC25A51*-KD cells transfected with a cDNA encoding the yeast mitochondrial NAD$^+$ transporter NDT1 (KD + NDT1). **d**, NAD$^+$ content of mitochondria isolated from HEK 293T control cells and cells stably overexpressing SLC25A51 (OE) before and after a 20-min incubation with 1 mM NAD$^+$. In **a**–**d**, $n = 3$ independent experiments. **e**, HeLa cells were transfected 3 days in advance with non-targeting siRNA (siNT) or siRNA targeting *SLC25A51* (siA51) or *NAMPT* (siNampt) and mitochondrial free NAD$^+$ levels were measured after 16 h of nicotinamide riboside (NR) treatment ($n = 3$). **f**, HEK 293 cells stably expressing *A. thaliana* NDT2–Flag, SLC25A32–Flag, and SLC25A51–Flag (**f**) or SLC25A52–Flag (**g**) were transfected with mitochondrially targeted eGFP (mito-eGFP) or the catalytic domain of PARP1 (mito–PARP1cd). Mitochondrial PARylation levels reflect mitochondrial NAD$^+$ availability. **h**, Mitochondrial NAD$^+$ content after 7 h of treatment with doubly isotopically labelled NaR. **i**, **j**, Whole-cell (**i**) and mitochondrial fraction (**j**) labelling patterns normalized to total ion counts in wild type to reflect relative abundance of NAD$^+$ after NaR treatment ($n = 3$). *n* represents biologically independent replicates unless otherwise indicated. Data are mean ± s.e.m. *P* values were determined by unpaired, two-tailed Student's *t*-test. $^*P < 0.05$, $^{**}P < 0.01$ and $^{***}P < 0.001$ versus untreated, wild-type $M + 0$; $^{\#\#\#}P < 0.001$ versus control + NAD$^+$, wild-type $M + 1$; $^{\wedge\wedge\wedge}P < 0.001$ versus wild-type $M + 2$ (exact *P* values are provided in the Source Data).

Exogenous NAD$^+$ increased the matrix NAD$^+$ content in control mitochondria and in mitochondria that had low NAD$^+$ content owing to inhibition of NAD$^+$ synthesis with FK866 in the parent cells (Fig. 3a, b, Extended Data Fig. 3a). This effect was specific to NAD$^+$, as it was not recapitulated with either nicotinamide or NMN (Extended Data Fig. 3b). Moreover, addition of excess nicotinamide or NMN did not compete with uptake of NAD$^+$ (Extended Data Fig. 3c). In mitochondria isolated from SLC25A51-deficient cells, exogenous NAD$^+$ did not increase the matrix NAD$^+$ content (Fig. 3a, b). Further, re-expression of SLC25A51 in SLC25A51-depleted or SLC25A51-KO cells restored uptake of exogenous NAD$^+$ (Fig. 3a, b). Yeast NDT1, a bona fide mitochondrial NAD$^+$ transporter[2], similarly rescued NAD$^+$ uptake in SLC25A51-deficient cells (Fig. 3c). This indicates that a lack of transport activity is probably the defect limiting mitochondrial NAD$^+$ accumulation in the absence of SLC25A51. Consistent with a direct role for SLC25A51 in NAD$^+$ transport, overexpression was sufficient to increase uptake of exogenous NAD$^+$ into isolated mitochondria (Fig. 3d). Finally, we used a mitochondrially targeted biosensor in intact cells to show that incubation with the NAD$^+$ precursor nicotinamide riboside was sufficient to restore mitochondrial NAD$^+$ levels in an SLC25A51-dependent manner (Fig. 3e). Together, these data indicate that the ability of mitochondria to import NAD$^+$ is dependent on the expression of either SLC25A51 or a protein with NAD$^+$ transporter activity.

To further investigate the capabilities of SLC25A51 and SLC25A52 to mediate mitochondrial NAD$^+$ transport in intact cells, we used a mitochondrially targeted poly ADP-ribose polymerase (mito–PARP1cd)[29]. This reporter system is based on the continuous consumption of mitochondrial NAD$^+$ and its preference for automodification with poly ADP-ribose (PAR). Thus, the steady-state level of PAR is an indication of the ability of mitochondria to replenish the NAD$^+$ pool. Overexpression of SLC25A51 or SLC25A52 markedly enhanced the signal of the mitoPARPcd reporter, similar to the effect of the *Arabidopsis thaliana* NAD$^+$ transporter AtNDT2 (Fig. 3f, g). Expression of SLC25A32—the mammalian mitochondrial carrier most homologous to AtNDT2—had no effect, as previously reported[5].

Nicotinic acid riboside (NaR) is converted to NAD$^+$ via the cytosolic enzyme NAD$^+$ synthase. By isotopically labelling both the nicotinic acid and ribose moieties, we can monitor a pool of NAD$^+$ synthesized in the cytosol, which we previously demonstrated is able to enter the mitochondria[15]. We incubated wild-type and SLC25A51-KO HAP1 cells with double-labelled NaR and measured the appearance of double-labelled NAD$^+$ in the mitochondria. Whereas NaR increased the total abundance of mitochondrial NAD$^+$ in wild-type cells, it had no effect in SLC25A51-KO cells (Fig. 3h). Whole-cell NAD$^+$ pools were labelled to a similar extent in both cell populations (Fig. 3i), but as expected, a substantial portion of the labelled NAD$^+$ entered the mitochondria only in wild-type cells and not in the SLC25A51-KO cells (Fig. 3j). Notably, the small amount of NAD$^+$ that was present in the KO cells was still partially labelled, suggesting that even the residual NAD$^+$ is taken up directly, whether via SLC25A52 or another mechanism, and not synthesized within the mitochondria (Extended Data Fig. 3d).

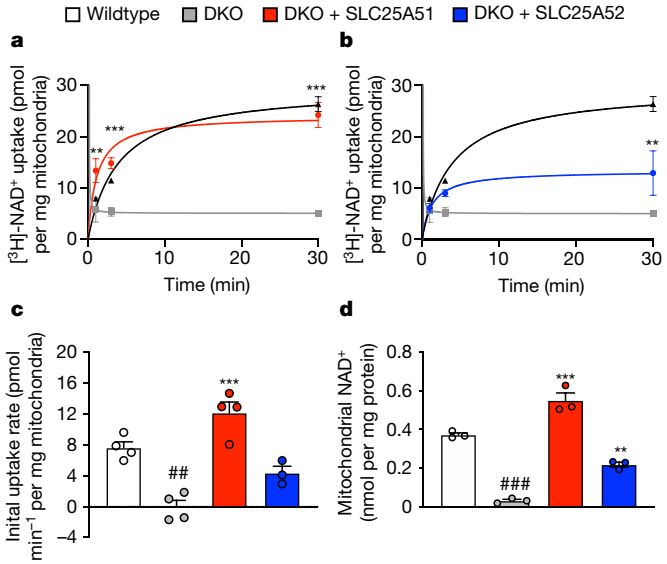

Fig. 4 | SLC25A51 is sufficient for transport of NAD$^+$ into yeast mitochondria lacking the endogenous transporters NDT1 and NDT2. a, **b**, [^{3}H]NAD$^+$ uptake measured in isolated mitochondria from wild-type ($n = 4$ independent experiments), DKO yeast cells ($n = 4$ independent experiments) or DKO yeast cells with overexpression of SLC25A51 ($n = 4$ independent experiments) (**a**) or DKO yeast cells with overexpression of SLC25A52 ($n = 3$ independent experiments) (**b**). The grey line indicates mean radioactivity in DKO samples. *P* values were determined by a two-way ANOVA with multiple comparisons analysis using Dunnett's method. **c**, Initial rates of NAD$^+$ uptake into isolated yeast mitochondria ($n = 4$ independent experiments for wild type, DKO and DKO + SLC25A51; $n = 3$ for DKO + SLC25A52). **d**, NAD$^+$ content of isolated yeast mitochondria ($n = 3$ biological independent replicates). *P* values were determined by one-way ANOVA with multiple comparisons using Tukey's method. Data are mean ± s.e.m. $^{**}P < 0.01$ and $^{***}P < 0.001$ versus DKO, $^{\#\#}P < 0.01$ and $^{\#\#\#}P < 0.001$ versus wild type (exact *P* values are provided in the Source Data).

SLC25A51 complements deficiency of NDT1 and NDT2

To investigate the function of SLC25A51 in a system that lacks transport activity, we developed a recombinant assay using [^{3}H]NAD$^+$ in yeast with deletions of the genes encoding both established mitochondrial NAD$^+$ transporters, NDT1 and NDT2 (DKO) (Extended Data Fig. 4a–e). We isolated mitochondria from either wild-type or DKO yeast in mid-exponential growth and incubated them with 100 µM NAD$^+$ ([^{3}H]NAD$^+$ traced). Wild-type mitochondria readily imported NAD$^+$, with an initial rate of 7.6 ± 1.5 pmol min^{-1} (mean ± s.d.) (Fig. 4a–c, Extended Data Table 2). There was minimal uptake of NAD$^+$ by DKO mitochondria over 30 min. Ectopic expression of human SLC25A51 in the DKO strain fully rescued mitochondrial NAD$^+$ uptake (initial rate 12.1 ± 2.8 pmol min^{-1}; mean ± s.d.), and SLC25A52 provided a partial rescue (initial rate 4.3 ± 1.5 pmol min^{-1}; mean ± s.d.) (Fig. 4a–c, Extended Data Table 2). As expected, excess unlabelled NAD$^+$ competed with import of [^{3}H]NAD$^+$ into DKO cells rescued with SLC25A51 (Extended Data Fig. 5a). However, the initial rate of uptake was not significantly altered by up to 500 µM NMN or 100 µM NADH (Extended Data Fig. 5b, c, Extended Data Table 2), supraphysiological concentrations exceeding free cytosolic levels by 1–2 orders of magnitude[21,30–32]. Consistent with the ability of human SLC25A51 and SLC25A52 to transport NAD$^+$ into mitochondria, expression of either transporter in the DKO strain was sufficient to restore mitochondrial NAD$^+$ levels (Fig. 4d). Although there is still no evidence that reconstituted SLC25A51 is sufficient to transport NAD$^+$ in an isolated system, these experiments demonstrate that it can functionally replace bona fide mitochondrial NAD$^+$ transporters. To define kinetic parameters for SLC25A51, we determined the abundance of SLC25A51 in mitochondrial preparations. We obtained mass spectrometry data for 15 mitochondrial proteins of similar molecular weights whose levels did not fluctuate across experimental conditions. Peptide counts were mapped onto a meta-dataset of absolute yeast protein abundances[33] to obtain a standard curve that was then used to estimate the concentration of SLC25A51 in each sample (Extended Data Fig. 5d), yielding a value of approximately 475 ng (approximately 14 pmol) of SLC25A51 per milligram of isolated mitochondria. We measured NAD$^+$ uptake by SLC25A51 at 1 min, 3 min and 30 min using a range of NAD$^+$ concentrations: 100 µM, 200 µM, 300 µM, 500 µM and 1,000 µM NAD$^+$ (Extended Data Fig. 5e). Initial rates were interpolated from the linear portions of the curves between 0.1–0.2 min. We plotted mean initial rates against NAD$^+$ concentrations in a double reciprocal (Lineweaver–Burk) plot and used the Michaelis–Menten equation to determine an apparent Michaelis constant (K_M) for NAD$^+$ transport by SLC25A51 of approximately 200 ± 60 µM and an apparent maximal velocity (V_{max}) of approximately 1,200 ± 300 pmol s^{-1} (Extended Data Fig. 5f). Together, these data demonstrate that human SLC25A51 and human SLC25A52 can directly transport NAD$^+$ into the mitochondrial matrix.

Conclusion

Despite the central role of NAD$^+$ in mitochondrial metabolism, the mechanism by which mammalian organelles obtain this dinucleotide has never been elucidated[9,15]. Here we have shown that SLC25A51 and its paralogue, SLC25A52, are both capable of mediating mitochondrial uptake of NAD$^+$, and that SLC25A51 is required for the maintenance of normal mitochondrial NAD$^+$ levels in human cells. Although these data do not exclude the possibility that other modes of mitochondrial NAD$^+$ replenishment exist, the essential nature of SLC25A51 across several cell lines suggest that direct SLC25A51-mediated uptake is a major mechanism responsible for the generation of the mitochondrial NAD$^+$ pool in mammals.

Online content

Any methods, additional references, Nature Research reporting summaries, source data, extended data, supplementary information, acknowledgements, peer review information; details of author contributions and competing interests; and statements of data and code availability are available at https://doi.org/10.1038/s41586-020-2741-7.

1. Palmieri, F. et al. Molecular identification and functional characterization of *Arabidopsis thaliana* mitochondrial and chloroplastic NAD$^+$ carrier proteins. *J. Biol. Chem.* **284**, 31249–31259 (2009).
2. Todisco, S., Agrimi, G., Castegna, A. & Palmieri, F. Identification of the mitochondrial NAD$^+$ transporter in *Saccharomyces cerevisiae*. *J. Biol. Chem.* **281**, 1524–1531 (2006).
3. Berger, F., Ramírez-Hernández, M. H. & Ziegler, M. The new life of a centenarian: signalling functions of NAD(P). *Trends Biochem. Sci.* **29**, 111–118 (2004).
4. Yang, H. et al. Nutrient-sensitive mitochondrial NAD+ levels dictate cell survival. *Cell* **130**, 1095–1107 (2007).
5. VanLinden, M. R. et al. Subcellular distribution of NAD$^+$ between cytosol and mitochondria determines the metabolic profile of human cells. *J. Biol. Chem.* **290**, 27644–27659 (2015).
6. Wang, T. et al. Identification and characterization of essential genes in the human genome. *Science* **350**, 1096–1101 (2015).
7. Bertomeu, T. et al. A high-resolution genome-wide CRISPR/Cas9 viability screen reveals structural features and contextual diversity of the human cell-essential proteome. *Mol. Cell. Biol.* **38**, e00302-17 (2017).
8. Yoshino, J., Baur, J. A. & Imai, S. I. NAD$^+$ intermediates: the biology and therapeutic potential of NMN and NR. *Cell Metab.* **27**, 513–528 (2018).
9. Cambronne, X. A. et al. Biosensor reveals multiple sources for mitochondrial NAD$^+$. *Science* **352**, 1474–1477 (2016).
10. Pittelli, M. et al. Inhibition of nicotinamide phosphoribosyltransferase: cellular bioenergetics reveals a mitochondrial insensitive NAD pool. *J. Biol. Chem.* **285**, 34106–34114 (2010).
11. Sims, C. A. et al. Nicotinamide mononucleotide preserves mitochondrial function and increases survival in hemorrhagic shock. *JCI Insight* **3**, 120182 (2018).
12. Titus, S. A. & Moran, R. G. Retrovirally mediated complementation of the glyB phenotype. Cloning of a human gene encoding the carrier for entry of folates into mitochondria. *J. Biol. Chem.* **275**, 36811–36817 (2000).

13. Spaan, A. N. et al. Identification of the human mitochondrial FAD transporter and its potential role in multiple acyl-CoA dehydrogenase deficiency. *Mol. Genet. Metab*. **86**, 441–447 (2005).
14. Berger, F., Lau, C., Dahlmann, M. & Ziegler, M. Subcellular compartmentation and differential catalytic properties of the three human nicotinamide mononucleotide adenylyltransferase isoforms. *J. Biol. Chem*. **280**, 36334–36341 (2005).
15. Davila, A. et al. Nicotinamide adenine dinucleotide is transported into mammalian mitochondria. *eLife* **7**, e33246 (2018).
16. Fletcher, R. S. et al. Nicotinamide riboside kinases display redundancy in mediating nicotinamide mononucleotide and nicotinamide riboside metabolism in skeletal muscle cells. *Mol. Metab*. **6**, 819–832 (2017).
17. Nikiforov, A., Dölle, C., Niere, M. & Ziegler, M. Pathways and subcellular compartmentation of NAD biosynthesis in human cells: from entry of extracellular precursors to mitochondrial NAD generation. *J. Biol. Chem*. **286**, 21767–21778 (2011).
18. Hikosaka, K. et al. Deficiency of nicotinamide mononucleotide adenylyltransferase 3 (nmnat3) causes hemolytic anemia by altering the glycolytic flow in mature erythrocytes. *J. Biol. Chem*. **289**, 14796–14811 (2014).
19. Yamamoto, M. et al. Nmnat3 is dispensable in mitochondrial NAD level maintenance in vivo. *PLoS ONE* **11**, e0147037 (2016).
20. Uhlén, M. et al. Proteomics. Tissue-based map of the human proteome. *Science* **347**, 1260419 (2015).
21. Sallin, O. et al. Semisynthetic biosensors for mapping cellular concentrations of nicotinamide adenine dinucleotides. *eLife* **7**, e32638 (2018).
22. Blomen, V. A. et al. Gene essentiality and synthetic lethality in haploid human cells. *Science* **350**, 1092–1096 (2015).
23. Hart, T. et al. High-resolution CRISPR screens reveal fitness genes and genotype-specific cancer liabilities. *Cell* **163**, 1515–1526 (2015).
24. Agerholm, M. et al. Perturbations of NAD^+ salvage systems impact mitochondrial function and energy homeostasis in mouse myoblasts and intact skeletal muscle. *Am. J. Physiol. Endocrinol. Metab*. **314**, E377–E395 (2018).
25. Frederick, D. W. et al. Loss of NAD homeostasis leads to progressive and reversible degeneration of skeletal muscle. *Cell Metab*. **24**, 269–282 (2016).
26. Rustin, P. et al. Fluxes of nicotinamide adenine dinucleotides through mitochondrial membranes in human cultured cells. *J. Biol. Chem*. **271**, 14785–14790 (1996).
27. Agrimi, G. et al. Deletion or overexpression of mitochondrial NAD^+ carriers in *Saccharomyces cerevisiae* alters cellular NAD and ATP contents and affects mitochondrial metabolism and the rate of glycolysis. *Appl. Environ. Microbiol*. **77**, 2239–2246 (2011).
28. Floyd, B. J. et al. Mitochondrial protein interaction mapping identifies regulators of respiratory chain function. *Mol. Cell* **63**, 621–632 (2016).
29. Dölle, C., Niere, M., Lohndal, E. & Ziegler, M. Visualization of subcellular NAD pools and intra-organellar protein localization by poly-ADP-ribose formation. *Cell. Mol. Life Sci*. **67**, 433–443 (2010).
30. Trammell, S. A. & Brenner, C. Targeted, LCMS-based metabolomics for quantitative measurement of NAD^+ metabolites. *Comput. Struct. Biotechnol. J*. **4**, e201301012 (2013).
31. Zhang, Q., Piston, D. W. & Goodman, R. H. Regulation of corepressor function by nuclear NADH. *Science* **295**, 1895–1897 (2002).
32. Zhao, Y. et al. SoNar, a highly responsive NAD^+/NADH sensor, allows high-throughput metabolic screening of anti-tumor agents. *Cell Metab*. **21**, 777–789 (2015).
33. Ho, B., Baryshnikova, A. & Brown, G. W. Unification of protein abundance datasets yields a quantitative *Saccharomyces cerevisiae* proteome. *Cell Syst*. **6**, 192–205 (2018).

Methods

Cell culture

HEK 293T (ATCC: CRL-3216), HEK 293 (ATCC: CRL-1573), HeLa (ATCC: CCL-2) and U2OS (ECACC: 92022711) cells were cultured in either Dulbecco's modified Eagle's medium (DMEM) containing 4.5 g l^{-1} glucose, 1 mM sodium pyruvate and 4 mM L-glutamine with supplemented with 10% fetal bovine serum and 1× penicillin–streptomycin, or a custom DMEM formulation without antibiotics or niacinamide for nicotinamide riboside (3-(aminocarbonyl)-1-β-D-ribofuranosyl-pyridinium, CAS: 1341-23-7) supplementation assays. HAP1 wild-type (Horizon Discovery: C631) and HAP1 SLC25A51-KO 4-bp deletion (Horizon Discovery: HZGHC001927c010) cells were cultured in Iscove's modified Dulbecco's culture medium supplemented with 10% fetal bovine serum and 1× penicillin–streptomycin. Low-passage J1 mouse embryonic stem cells (ATCC: SCRC-1010) were cultured in DMEM containing 4.5 g l^{-1} glucose without pyruvate (Sigma, D5796), 20% fetal bovine serum (Sigma, 12306C), 1× EmbryoMax Nucleoside Mix (Millipore, ES-008D), 1× Non-Essential Amino Acids Mix (Millipore, MS-001-C), 100 μM β-mercaptoethanol (Sigma, M3148) and 7×10^6 U recombinant mouse Leukaemia Inhibitory Factor (Millipore, ESG1107). Cells were grown at 37 °C with 5% CO_2. After stable depletion or deletion of SLC25A51, medium was supplemented with 50 μg ml^{-1} uridine (1-[(2R,3R,4S,5R)-3,4-dihydroxy-5-(hydroxymethyl)oxolan-2-yl]pyrimidine-2,4-dione, CAS: 58-96-8) to improve cellular viability. To deplete NAD^+, cells were treated with 100 nM FK866 (*N*-[4-(1-benzoyl-4-piperidinyl)butyl]-3-(3-pyridinyl)-2E-propenamide, CAS: 658084-64-1) for 18–24 h. All cell lines were routinely checked for mycoplasma.

Generation of NAD^+ sensor cell lines

Clonal HeLa ^{mito}cpVenus and HeLa ^{mito}Sensor cell lines were generated by lentiviral transduction of HeLa cells (ATCC: CCL-2) with virus encoding ^{mito}cpVenus or ^{mito}Sensor at a MOI of approximately one. Stable integration was selected with 2.5 μg ml^{-1} puromycin ((2S)-2-amino-*N*-[(2S,3S,4R,5R)-5-[6-(dimethylamino)purin-9-yl]-4-hydroxy-2-(hydroxymethyl)oxolan-3-yl]-3-(4-methoxyphenyl)propanamide, CAS: 58-58-2) for 2 weeks and individual clones were then isolated by dilution plating. Once colonies were established, 10 clonal lines were screened to confirm fluorescence and responses to FK866 treatment (10 nM, 16 h).

A U2OS and HEK 293 FlpIn T-Rex cell lines were generated as previously described[34]. The Flp-In T-Rex System (ThermoFisher Scientific) was used to generate inducible U2OS and HEK 293 Flp-In cell lines that express the NAD^+–Snifit in the mitochondria. pcDNA5-FRT-Cox8-SPR-Halo-p30-SNAP[19] and the Flp recombinase (pOG44) were co-transfected into the host FlpIn cell line following the manufacturer's instructions. Homologous recombination between the FRT sites in pcDNA5-FRT-Cox8-SPR-Halo-p30-SNAP and the host cell chromosome, catalysed by the Flp recombinase expressed from pOG44, produced stable and inducible U2OS and HEK 293 FlpIn cells. Cells were single-cell sorted before use.

shRNA and siRNA knockdown

Cells were transduced with lentivirus encoding shRNA targeting against human *SLC25A51* (Sigma, Mission shRNA). shRNA sequences used are: TRCN0000060234, CCGGGCACTTATGTTTGGTCTGTATCTCGAGATACAGACCAAACATAAGTGCTTTTTG; TRCN0000060235, CCGGGCAACTTATGAGTTCTTGTTACTCGAGTAACAAGAACTCATAAGTTGCTTTTTG; TRCN0000060237, CCGGGCACTGAAATGTCATGGAATTCTCGAGAATTCCATGACATTTCAGTGCTTTTTG. Non-targeting control shGFP targeting sequence: GCAAGCTGACCCTGAAGTTCAT3.

To generate stable knockdown cell lines, cells were selected with 2 μg ml^{-1} puromycin. Both gene expression and mitochondrial NAD^+ levels were used to validate targeting sequences (shRNA1- TRCN0000060234), (shRNA2- TRCN0000060235), and (shRNA3-TRCN0000060237). For human cell lines, TRCN0000060235 was used in figures simply referencing knockdown (KD). All of the analyses were conducted before the fifth passage after transduction.

Mouse shRNA against *Slc25a51*. To transiently deplete SLC25A51 expression and measure mitochondrial free NAD^+, J1 mouse embryonic stem cells were co-transfected using linear polyethylenimine (MW 250,000) with plasmids encoding shRNA targeting mouse *Slc25a51* and either ^{mito}cpVenus-IRES-puromycinR or ^{mito}Sensor-IRES-puromycinR expressed from an EF1α promoter. Plasmids were transfected at a ratio of 3:1 shRNA:sensor. The shRNA or control shFF2 (targeting firefly luciferase) hairpins were flanked by microRNA-30 sequences and constitutively expressed via the UBC promoter from the 3′UTR of a puromycin-resistance cassette. Two days post-transfection, cells were selected with 1 μg ml^{-1} puromycin for an additional 48 h.

Mouse *Slc25a51* hairpin sequence: GGTATATTGCTGTTGACAGTGAGCGAGGCCTTCGAGGGCCCATTAAGGTAGTGAAGCCACAGATGTACCTTAATGGGCCCTCGAAGGCATGCCTACTGCCTCGGACTTC; non-targeting control shFF2 (firefly luciferase #2) hairpin: GGTATATTGCTGTTGACAGTGAGCGAugguccaaccgacuaauacagTAGTGAAGCCACAGATGTActgtattagtcggttggaccaaTGCCTACTGCCTCGGACTTC.

siRNA knockdown. siGENOME siRNAs targeting human *SLC25A51* (D-007358-01, D-007358-02), *NAMPT* (D-004581-01) and non-targeting Scramble controls (D-001206-14) were obtained from Dharmacon RNAi Technologies and resuspended at 20 μM in 10 mM Tris pH 8.0 buffer. Lipofectamine RNAiMax transfection reagent (ThermoFisher Scientific) was used to transfect siRNA into cells. Cells were grown in DMEM complete media and incubated for 72 h after treatment.

Expression plasmids

Human cDNA encoding SLC25A51 (NCBI: NM_033412) and SLC25A52 (NCBI: NM_001034172) were either purchased from Origene (*SLC25A51*: RC203348 or MR204144; SLC25A52: RC215808) or synthesized as double-stranded DNA fragments. Synthesized sequences are either codon-optimized for expression in *Saccharomyces cerevisiae* or mammals. cDNA encoding NDT1 was obtained with gene-specific PCR from genomic DNA of BY4742 and expressed from its endogenous promoter. These genes were either cloned into pRS415 with HiFi assembly, or into pENTR-D-Topo (Gateway System, ThermoFisher Scientific). pENTR constructs were recombined using LR Clonase II into mammalian expression vectors.

Analysis of gene expression

RNA was isolated using the Qiagen RNeasy Mini Kit (Qiagen, 74104) and cDNA was generated using the Applied Biosystems High-Capacity cDNA Reverse Transcription Kit (Applied Biosystems, 4368814). quantitative PCR (qPCR) analysis was conducted following the manufacturer's instructions (Power Sybr, ThermoFisher Scientific, 4367659). Human 18S RNA was used as a house keeping control. To calculate fold change in mRNA expression, the $2^{-\Delta\Delta Ct}$ method was used. Primers were: yeast-codon optimized *SLC25A51* forward, ATAGGTGGCGAGTTTCAGAGTTT, reverse, TGAACGGTGATAGTTTAGGTGGG; yeast codon-optimized *SLC25A52* forward, CCATCACCTATCCGATCCAGAAG, reverse, TGGTGGCAGAATTCCTCTGTAAA; endogenous human *SLC25A51* mRNA, forward, TACCAACACTTACCAGGCTTTCA, reverse, CAAGACATTGCTGAGTCCATTCC or forward, CGCTGATGGGAAATCCAGTTA, reverse, CTGGAGTTTGGCAGGATGATAG; human *SLC25A52* mRNA, forward, ATGGACTCGGGAAGAGAGAA, reverse, CTGGAGTTTGGCAGGATGATAG); human 18S mRNA, forward, TTGACGGAAGGGCACCACCAG, reverse, GCACCACCACCCACGGAATCG.

Lysis and western blotting

Cells were washed with ice-cold PBS and lysed directly in either RIPA buffer (Cell Signaling, 9806) with Halt Protease and Phosphatase

Inhibitor (ThermoScientific, 78442) or 2× Laemmli sample buffer containing DTT. Protein samples were electrophoresed on 4–12% Bis-Tris protein gels (Invitrogen) or 10% Mini-PROTEAN TGX precast gel (Bio-Rad) and transferred to 0.45 µm nitrocellulose or PVDF membrane (Bio-Rad). Membranes were blocked with 5% BSA or 5% milk in Tris-buffered saline (TBS) pH 7.6 containing 0.1% (v/v) Tween-20 (TBST) or LiCOR blocking buffer. Antibodies were prepared in 1% BSA or 1:1 LiCOR Blocking Buffer in TBST. Dilutions were as follows: anti-SLC25A51 (ProSci, 55-424, 1:200), anti-Flag M2 (Sigma, F1804, 1:3,000), anti-α-tubulin (Sigma, T9026, 1:3,000), anti-total OXPHOS (Abcam, ab110413, 1:2,000), anti-TOM20 (Santa Cruz Biotechnology, sc-17764), anti-PAR 10H (Enzo, LX-804-220-R100, 1:6,000), anti-GFP JL-8 (Takara Clontech, 632381, 1:15,000), anti-SC2 (Novus Bio, NBP1-92465, 1:1,000), anti-actin (Abcam, ab14128, 1:1,000), anti-MTC02 (Abcam, ab9479, 1:1,000), anti-CoxIV (Abcam, ab33985, 1:1,000), anti-β-tubulin (Sigma, T5293, 1:10,000) and anti-mouse IgG H&L IRDye 800CW (Abcam, ab216773, 1:10,000), IRDye 680RD Goat anti-Mouse IgG (LiCOR, 926-68070, 1:12,000), IRDye 800CW Donkey anti-Rabbit IgG (LiCOR, 926-32213, 1:12,000). Total protein loading was determined using Revert 700 Total Protein Dye (LiCOR, 926-11010). Membranes were imaged using a LiCOR Odyssey Clx or a ChemiDoc XRS+ imaging system (Bio-Rad).

Overexpression of SLC25A51

SLC25A51 was cloned into pAd/CMV/V5-dest (Invitrogen, V49320) from the entry plasmid Gateway PLUS shuttle clone for *SLC25A51* (NM_033412.3) (Genecopoeia, GC-T0831) by recombination using LR Clonase II (Gateway system; Invitrogen, 11791020. pAd/CMV/V5-dest containing *SLC25A51* was used to generate adenovirus in HEK 293T cells. Adenovirus titre was determined, and cells were treated with adenovirus encoding SLC25A51 at an MOI ranging from 2 to 6. Sixteen to twenty hours after transduction, the virus-containing medium was removed, and new medium was added. To restore SLC25A51 expression in SLC25A51 knockdown cells, a plasmid encoding mouse *Slc25a51* was transfected into cells using Fugene 6 (1:3 DNA:Fugene ratio) (Promega, E269A). Cells were transfected or transduced 48–72 h before the experiment. A stable SLC25A51-overexpression cell line was generated using genomic integration with lentivirus encoding pCMV-Flag-HA-SLC25A51-IRES-puro in HEK 293T cells. After transduction, the cell line was selected using puromycin as described above.

NAD^+ measurement in extracts

Cells and mitochondria were extracted with ice-cold 0.6 N perchloric acid. NAD^+ was measured after extraction by an enzymatic cycling assay in a 96-well format. Standards or diluted sample extracts (at least 1:10 in in 100 mM phosphate buffer, pH 8.0) were combined with 95 µl of cycling mixture (2% ethanol, 100 µg/ml alcohol dehydrogenase, 10 µg ml^{-1} diaphorase, 20 µM resazurin, 10 µM flavin mononucleotide, 10 mM nicotinamide, 0.1% BSA in 100 mM phosphate buffer, pH 8.0). The rate of resorufin accumulation was measured by comparing fluorescence excitation at 544 nm and emission at 590 nm before and after incubation of the cycling reaction for 15 min at room temperature.

Mitochondrial NAD^+ measurements using the NAD^+ biosensor and semisynthetic NAD^+-Snifit

Clonal Hela lines stably expressing ^{mito}cpVenus or ^{Mito}Sensor were seeded into a 24-well plate one day before transfection (about 20,000–50,000 cells per well). The cells were transfected with mitochondrial carrier family constructs, (pCMV-Flag-HA-IRES-puro plasmids encoding *NDT1* NP_012260.1, *SLC25A32* NP_110407.2, *SLC25A33* NP_115691.1, *SLC25A36* NP_001098117.1, *SLC25A51* NP_219480.1 or *SLC25A52* NP_001029344.4) (0.5 µg DNA per well), using 2.5 µl of polyethylenimine solution (1 mg ml^{-1}) in 100 µl of Opti-MEM or transfected with 20 nM siRNA,1 µl Lipofectamine RNAiMax in 100 µl Opti-MEM. Cells were grown in DMEM complete medium and incubated for 48–72 h. For nicotinamide riboside treatment, cells were treated with 100 µM NR in complete DMEM without nicotinamide 16 h before analysis. Measurements of mitochondrial NAD^+ using the NAD^+ biosensor has previously been described[35]. In brief, HeLa ^{mito}cpVenus and HeLa ^{mito}Sensor cells were collected in ice-cold DMEM and kept cold until analysis. Data was collected on a NovoCyte flow cytometer using the following parameters: excitation 488 nm, emission 530 ± 30 nm and excitation 405 nm, emission 530 ± 30 nm. Cells were gated to exclude debris, a standard doublet-exclusion was performed, and 10,000 fluorescent cells were analysed per condition. Ratiometric 488/405 nm fluorescence values were obtained for each cell using the derived function on FlowJo v.10.

U2OS and HEK 293 T-Rex Flp-In cells with an inducible NAD^+–Snifit sensor in the mitochondria were plated at 5×10^4 cells per ml in a 24-well plate (TPP, 92024). Sensor expression was induced by the addition of doxycycline (4S,4aR,5S,5aR,6R,12aR)-4-(dimethylamino)-1,5,10,11,12a-pentahydroxy-6-methyl-3,12-dioxo-4a,5,5a,6-tetrahydro-4H-tetracene-2-carboxamide, Cas: 564-25-0) (200 ng ml^{-1}). After 24 h, the cells were transfected with either cDNA encoding SLC25A51, SLC25A52 or an empty pcDNA3.1 vector using Fugene 6 (1:1.5 DNA:Fugene ratio, 0.5 µg DNA per well) Promega, E269A. At 48 h, the cells were labelled with CP-TMR-C6-SMX (500 nM) and Halo-SiR (200 nM)[21] for 16 h. The cells were resuspended in 2% FBS in PBS, filtered and subjected to flow cytometry analysis. Flow cytometry data were recorded on a FACS Melody (BD Bioscience) or an LSR II (BD Bioscience) using the following settings: TMR (excitation 561 nm, emission 582 ± 15 nm), FRET (excitation 561 nm, emission 697 ± 58 nm) and SiR (excitation 640 nm, emission 660 ± 10 nm). Cells were gated to exclude debris, a standard doublet-exclusion was performed, and 10,000 fluorescent cells were analysed per condition. The data were analysed with FlowJo v.10 software.

Respiration assays

Cells (80,000 cells per well) were plated into a well of a Seahorse XF 96 well culture plate and cultured overnight. After 16–20 h the cells media was changed to XF DMEM Medium containing 10 mM glucose, 1 mM sodium pyruvate and 2 mM L-glutamine and incubated for 1 h at 37 °C without CO_2. Cell respiration was measured using a Seahorse XF96e Analyzer. Cells were treated with 1.5 µM oligomycin (an ATP synthase inhibitor, 4-ethyl-11,12,15,19-tetrahydroxy-6′-(2-hydroxypropyl)-5′,10,12,14,16,18,20,26,29-nonamethylspiro[24,28-dioxabicyclo[23.3.1]nonacosa-5,7,21-triene-27,2′-oxane]-13,17,23-trione, CAS: 579-13-5), 1.5 µM FCCP (a mitochondrial uncoupler, 2-[2-[4-(trifluoromethoxy)phenyl]hydrazinylidene]-propanedinitrile, CAS: 370-86-5), 0.5 µM rotenone/antimycin A (complex I and III inhibitors, rotenone: (1S,6R,13S)-16,17-dimethoxy-6-prop-1-en-2-yl-2,7,20-trioxapentacyclo[11.8.0.03,11.04,8.014,19]henicosa-3(11),4(8),9,14,16,18-hexaen-12-one. CAS: 83-79-4; antimycin a: [(2R,3S,6S,7R,8R)-3-[(3-Formamido-2-hydroxybenzoyl)amino]-8-hexyl-2,6-dimethyl-4,9-dioxo-1,5-dioxonan-7-yl] 3-methylbutanoate, CAS: 1397-94-0). Basal respiration is respiration before the addition of any drugs and maximum respiration is peak respiration after oligomycin and FCCP treatment.

To measure mitochondrial respiration, 7.5 µg per well mitochondria were plated on Seahorse XF 96-well culture plate by centrifuging for 20 min at 1,000*g*. Respiration of mitochondria was measured in MiRO5 respiration medium (110 mM sucrose, 20 mM HEPES, 10 mM KH_2PO_4, 20 mM taurine, 60 mM K-lactobionate, 3 mM $MgCl_2$, 0.5 mM EGTA, and 1 g l^{-1} fatty acid free BSA adjust pH to 7.2 with KOH) using a Seahorse XF96e Analyzer at 37 °C. To measure state 2 respiration 5 mM malate and 10 mM pyruvate were added. State 3 respiration was measured with the addition of 2 mM ADP. To inhibit complex V and block ATP generation, 1.5 µM oligomycin was added.

For assessing the consequences of NAD^+ depletion in mitochondria, respiration of isolated mitochondria (200 µg per chamber for Oroboros or 7.5 µg per well for Seahorse XF96e) was measured in MiRO5

respiration medium using an Oroboros high-resolution respirometer or Seahorse XF96e Analyzer at 37 °C. To measure state 2 respiration, 5 mM malate and 10 mM pyruvate were added. State 3 respiration was measured with the addition of 2 mM ADP. After stabilization of the state 3 reading, 1 mM NAD^+ was added to determine whether its addition could restore state 3 respiration in NAD^+ depleted mitochondria.

Cell proliferation assay

To measure cell proliferation, cells were plated at 10,000 cells per well into a 96-well plate. The CyQuant (Invitrogen, C7026) cell proliferation assay was conducted using the manufacturer's protocol to measure DNA content at 0 h and 96 h after plating the cells.

Mitochondrial membrane potential and mitochondrial content assays

Cells were loaded with either TMRE (Invitrogen, T669) to measure mitochondrial membrane potential or MitoTracker Deep Red (Cell Signaling, 8778S) to label mitochondria following the manufacturer's protocols. After loading, the cells were collected by trypsinization, resuspended in 2% FBS in PBS, filtered and subjected to flow cytometry analysis. Flow cytometry data were recorded on an LSR II (BD Bioscience) for 10,000 events. To measure mitochondrial membrane potential, fluorescence intensity data was collected using excitation 561 nm, emission 582 ± 15 nm. To control for TMRE loading, FCCP was added to collapse the mitochondrial membrane potential after collecting the baseline recording. The FCCP recording was subtracted from the baseline recording. To measure mitochondrial content in intact cells, the MitoTracker Deep Red fluorescence intensity data were collected using excitation 640 nm, emission 660 ± 10 nm.

Mammalian mitochondrial isolation

Cells were cultured on a 100-mm or 150-mm plate. For experiments in which mitochondria were depleted of NAD^+, the medium was changed the day before collection and the cells were treated with 100 nM FK866 for 18–24 h. Cells were collected by trypsinization. Mitochondria were isolated by homogenizing cells in 2 ml of mitochondrial isolation buffer (210 mM mannitol, 70 mM sucrose, 10 mM HEPES, 1 mM EGTA, 0.25% fatty acid free BSA, pH adjusted to 7.2 with KOH) using a dounce homogenizer (1,200 rpm, 20 strokes). Mitochondria were collected by differential centrifugation. Cell debris was spun down at 800*g* for 10 min and supernatant was transferred to a new tube. This was repeated until no cell debris pellet was present. Next the supernatant was spun at 11,000*g* for 15 min. The mitochondrial pellet was resuspended in 50–200 µl BSA-free mitochondrial isolation buffer.

Mammalian mitochondrial NAD^+ uptake

To measure mitochondrial NAD^+ uptake, isolated mitochondria (50–200 µg) were resuspended in MiR05 containing 5 mM malate and 10 mM pyruvate along with NAD^+ (1 mM) in a 1.5 ml Eppendorf tube. The reaction was agitated at 900 rpm and the tube was briefly opened every 10 min to allow for re-oxygenation. Mitochondria were pelleted by centrifugation (14,000*g* for 2 min). The mitochondrial pellet was washed 2 times with ice-cold mitochondrial isolation buffer before extracting in ice-cold 0.6 N perchloric acid for biochemical measurements of mitochondria NAD^+ content.

Labelled NaR and metabolomics

For the tracer studies, cells were treated with double-isotope labelled 0.1 mM NaR (double labelled with a ^{13}C label on the pyridine carboxyl group and a deuterium label on the ribose moiety) for 7 h in complete Iscove's modified Dulbecco's culture medium supplemented with 10% fetal bovine serum and 1× penicillin–streptomycin and 50 µg ml^{-1} uridine before extracting. The cells were then rapidly collected using trypsin and medium containing the label and were washed with ice-cold isolation buffer. Either cells or subsequently isolated mitochondria were collected for analysis.

Metabolites were extracted from pelleted mitochondria and whole cells using −80 °C, 80:20 methanol:water. Whole-cell and mitochondrial extracts were analysed by liquid chromatography coupled to a mass spectrometer (LC–MS). The LC–MS method used hydrophilic interaction chromatography (HILIC) coupled to the Q Exactive PLUS mass spectrometer (Thermo Scientific)[36]. The LC separation was performed on a XBridge BEH Amide column (2.1 mm × 150 mm, 2.5 µm particle size, 130 Å pore size, Waters). Solvent A was 95%: 5% H2O: acetonitrile with 20 mM ammonium bicarbonate, and solvent B was acetonitrile. The gradient was 0 min, 85% B; 2 min, 85% B; 3 min, 80% B; 5 min, 80% B; 6 min, 75% B; 7 min, 75% B; 8 min, 70% B; 9 min, 70% B; 10 min, 50% B; 12 min, 50% B; 13 min, 25% B; 16 min, 25% B; 18 min, 0% B; 23 min, 0% B; 24 min, 85% B; 30 min, 85% B. Other liquid chromatography parameters were: flow rate 150 ml min^{-1}, column temperature 25 °C, injection volume 10 ml and the autosampler temperature was 5 °C. The mass spectrometer was operated in both negative and positive ion mode for the detection of metabolites. Other mass spectrometry parameters were: resolution of 140,000 at m/z 200, automatic gain control (AGC) target at 3×10^6, maximum injection time of 30 ms and scan range of m/z 75–1,000. Raw LC–MS data were converted to mzXML format using the command line msconvert utility[37]. Data were analysed via MAVEN v.3.1 software, and all isotope labelling patterns were corrected for natural ^{13}C abundance using AccuCor[38]. To determine metabolites that were significantly changed, the fold change of metabolites was analysed with multiple *t*-tests and a false discovery rate (FDR) was calculated using the two-stage step-up method of Benjamini, Krieger and Yekutieli) with a desired FDR of 1%. A volcano plot was generated using Prism 8.0 comparing the −log(adjusted *P* value) to fold change. A heat map was generated using MetaboAnalyst 3.0[39]. To generate the heat map, the samples were normalized by the median and the data was log transformed. A hierarchical clustering heat map was produced using a Pearson correlation to determine distance and Ward's method for clustering analysis. *t*-test or ANOVA was used to determine top 30 metabolite changes.

Generation of stably transfected HEK 293 cells

Parental HEK 293 cells were cultivated in DMEM (high glucose) supplemented with 10% (v/v) fetal calf serum (FCS), 2 mM glutamine, 1 mM sodium pyruvate 100 U ml^{-1} penicillin and 100 µg ml^{-1} streptomycin. One day after transfection of 10^6 parental HEK 293 cells in a 6-well plate with 1 µg plasmid encoding C-terminally Flag–HA-tagged carriers using X-tremeGENE 9 transfection reagent (Merck Sigma XTG9-RO), one fifth of the cells were distributed onto a 10-cm dish and grown for 10 days in complete DMEM supplemented with 550 µg ml^{-1} G418 while replacing the medium every other day. A total of 350 surviving cells were seeded on a 10-cm dish for a first round of clonal selection. Subsequently, cell clones were transferred into a 24-well plate and further expanded. Cells stably expressing the transgene were identified by Flag-immunoblot analysis and subjected to another round of clonal selection.

Poly-ADP-ribose assisted detection of mitochondrial NAD^+

Parental HEK 293 cells and stably transfected HEK 293 cells expressing *A. thaliana* NDT2 (AtNDT2), human SLC25A32 (NM_030780), human SLC25A51 (NM_033412), and human SLC25A52 (NM_001034172) were grown in a 6-well plate and transfected with 1 µg plasmid encoding a mitochondrially targeted fusion construct composed of eGFP and the catalytic domain of PARP1 (mito–PARP1cd) using X-tremeGENE 9 transfection reagent. Cells transfected with the same construct lacking the PARP1cd portion (mito–eGFP) served as control. Thirty hours post transfection, cells were washed with 1 ml PBS before adding 130 µl lysis buffer (20 mM TrisHCl pH 7.4, 150 mM NaCl, 1% (v/v) SDS, 1 mM EDTA, 1 mM 3-aminobenzamide). After 10 passages of the lysates through a 23-gauge needle and determination of protein concentration using BCA assay (ThermoFisher, 23225), 50 µg of lysate were separated by reducing SDS-polyacrylamide gel electrophoresis in a 7% and 10% gel and

subjected to immunoblotting using anti-PAR, anti-Flag, anti-GFP, and anti-β-tubulin antibodies followed by incubation with HRP-conjugated goat anti-mouse secondary antibody. Overnight incubation at 4 °C was used for primary antibodies and 1 h incubation at room temperature for the secondary antibody. Horseradish peroxidase detection was performed using Super Signal West Dura Extended Duration Substrate (ThermoFisher, 34075) and a ChemiDoc XRS+ imaging system (Bio-Rad).

Generation of yeast strains

The *ndt2Δ::KanMX* targeted deletion strain in BY4742 (*MATα; his3Δ1; leu2Δ0; lys2Δ0; ura3Δ0*) background was purchased from the Yeast Knockout Collection through GE Healthcare (YSC6272-201917555) and confirmed via genomic PCR. The double *ndt1Δ ndt2Δ* knockout strain was generated by additional cassette replacement of *NDT1* with the HygMX cassette from pAG32. pRS415 or pRS415-based plasmids containing sc. *NDT1*, *SLC25A51* or *SLC25A52* were transformed using the LiAc method[40], selected for and maintained in SC-Leu media.

Yeast mitochondrial isolation

Mitochondria were isolated as previously described[41]. In brief, mitochondria were grown in 500 ml YPR (yeast extract, peptone, 2% raffinose) until the culture reached exponential phase. Raffinose was used as a carbon source instead of dextrose to promote respiration[42].These cultures were pelleted, washed and resuspended in zymolyase buffer (1.2 M sortbitol, 20 mM potassium phosphate, pH 7.4). The cell suspension was treated with zymolyase at 1 unit per ml of the original culture and shaken at 80 rpm at 30 °C for 30 min. After zymolyase treatment the spheroplasts were kept on ice. The spheroplasts were pelleted, washed and resuspended in homogenization buffer (0.6 M sorbitol, 10 mM Tris-HCl, pH 7.4, 1 mM EDTA (EDTA) 0.2% w/v BSA and protease inhibitors at 2×). For mass spectrometry analysis, BSA was omitted. The suspension was homogenized using 15 strokes of a 10 ml dounce homogenizer. The mitochondria were then isolated from the lysate using differential centrifugation. The mitochondria were stored on ice and in buffer containing sorbitol to preserve the osmolarity of the organelles (homogenization buffer). Isolated mitochondria were used within 3 h of isolation.

Uptake of [^{3}H]NAD$^+$ in isolated yeast mitochondria

Uptake was performed as previously described[43]. Isolated mitochondria (3 mg for 3 time points) were pelleted at 12,000*g* for 10 min at 4 °C. Protein concentrations were measured using absorbance at 280 nm. Mitochondrial pellets were maintained in sorbitol buffer until immediately before use. Pellets were resuspended in 50 µl suspension buffer (120 mM KCl, 5 mM KH_2PO_4, 1 mM EGTA, 3 mM HEPES pH 7.4, pH to 7.4 with KOH). The reaction was initiated by addition of 100 µl of respiration buffer (120 mM KCl, 5 mM KH_2PO_4, 1 mM EGTA, 3 mM HEPES pH 6.8) that included 1.5× substrate mix (1.5 mM ADP, 1.5 mM ATP, 30 mM succinate, 150 µM malate, 150 µM–1,500 µM NAD$^+$ as indicated, pH to 6.8 with KOH). Reaction buffer also included 0.3–3 nmol of [^{3}H]NAD$^+$, depending on relative NAD$^+$ concentration to maintain the ratio when varying the concentration of substrate. For competition assays, 0.3 nmol [^{3}H]NAD$^+$ was used. [^{3}H]NAD$^+$ was purchased from Moravek (1 mCi ml^{-1}). The total 1× reaction volume was 150 µl, yielding three 50 µl samples for 1, 3 and 30 min time points. Each time point was filtered through a 0.22-µm MCE filter using vacuum filtration and then washed with 5 ml suspension buffer. Washed filters were placed in a 7-ml scintillation vial and dissolved in 5 ml Filtron-X scintillation fluid. Scintillation vials were analysed using an LSC6500 liquid scintillation counter at 1 min per sample. Background signal from equivalent amounts of [^{3}H]NAD$^+$ incubated without mitochondria was subtracted. For calculating rates, mean background signal from the DKO strain was subtracted.

Quantitation of SLC25A51 abundance in yeast samples

Wild-type, double-knockout (*Δndt1 Δndt2*) and pRS415-TEF SLC25A51; *Δndt1 Δndt2* strains were grown in triplicate in 250 ml YPR to mid-exponential phase at 30 °C, 225 rpm. OD_{600} was used to estimate the cell concentrations of each culture so that 9×10^9 cells were used for each isolation. Mitochondria were isolated in the absence of BSA. After determining the yield of each mitochondrial preparation, 10 µg of mitochondria per sample were pelleted at 10,000*g* for 15 min at 4 °C. The mitochondrial pellet was lysed in 20 µl of 20 mM Tris pH 7.4, 200 mM NaCl, 20 mM C12M for 30 min at 4 °C. The lysate was centrifuged at 10,000*g* for 30 min at 4 °C and supernatant was immediately placed in 20 µl 2× Laemmli buffer and boiled at 95 °C for 5 min. The samples were resolved in a 10% Bis-Tris gel at 100 V for 20 min and stained with imperial stain. Gel sections between 25 kDa and 37 kDa were excised with a clean razorblade and treated with 50% ethanol, 50 mM ammonium bicarbonate for 30 min at room temperature. Gel cubes were then reduced and subjected to in-gel digest with trypsin. Peptide samples were extracted in acetonitrile and desalted before analysis on a Dionex LC and Orbitrap Fusion 1 for LC–MS/MS with a 2-h run time. Integrated peak intensities were mapped onto a known metadata set of absolute protein abundances[33] to interpolate an estimate of SLC25A51 abundance per mg of mitochondria. Selection of proteins used to generate the standard curve were uniquely mitochondrially localized, had consistent abundance across all experimental conditions, and had confirmed molecular weights between 25 and 37 kDa. Using the standard curve, the amount of SLC25A51 expressed was estimated to be about 3,000 molecules per cell. Calculated concentration of SLC25A51 in each uptake reaction was about 280 nM ± 40 nM SLC25A51 or about 480 ng ± 70 ng SLC25A51 per mg of mitochondria.

Immunofluorescence and imaging

Approximately thirty hours following transient transfected of either pCMV-Flag-HA-SLC25A51 or pCMV-Flag-HA-SLC25A52, HeLa cells seeded on coverslips were fixed using 4% paraformaldehyde (Electron Microscopy Sciences 15710) in PBS for 15 min at room temperature. Fixed cells were then washed in PBS, blocked, and permeabilized for 1 h at room temperature in 5% normal goat serum, 0.3% Triton X-100, PBS. Primary antibodies were diluted and incubated with cells overnight at 4 °C in 1% BSA, 0.3% Triton X-100, PBS. Rabbit anti-Flag (Cell Signaling Technologies, 14793, 1:500); mouse anti-MTC02 (Abcam, ab79479, 1:40). After washing, secondary antibodies were similarly diluted and incubated with cells for 1 h at room temperature. Goat anti-Mouse IgG–Alexa Fluor 488 (Invitrogen A-11001, 1:1,000); Goat anti-Rabbit IgG–Alexa Fluor 568 (Invitrogen A-11036, 1:1,000). Following three PBS washes, cells were mounted with Vectashield Hardset w/ DAPI (Vector Labs, H-100). Optical slices 0.11-µm thick were imaged using a Yokogawa W2 spinning disk confocal setup that includes 100mW 488 nm and 565 nm lasers, a 100× Olympus objective, and a Photonics Prime 95B sCMOS camera.

Mitochondrial volumetric analyses

For analyses of mitochondrial volume per cell, a *z*-stack series comprised of 0.11-µm optical slices that comprehensively covered the full depth of a single cell was captured and imported into Bitplain Imaris x64 (v.8.4.1) for assembly. Data for over 30 individuals per experimental condition were collected and analysed in a blinded fashion. Power analysis (alpha 0.05, beta 0.8) indicated that a sample size of 26 cells would be sufficient to observe differences with this confidence. Surfaces analysis was performed for each cell; surface detail was set to 0.1 µm. For thresholding, background subtraction (local contrast) was performed using a spherical diameter of 0.2 µm surrounding the identified surfaces. A volume filter was applied to analyse objects above 0.0184 µm^3. Data were collected for cumulative

volume per cell, number of disconnected puncta components per cell, and median volume of each disconnected unit. Data were analysed for statistical significance between conditions using GraphPad Prism v.8.2.0.

Statistics and reproducibility

All results are presented as mean ± s.e.m. as indicated. No statistical methods were used to predetermine sample size. The experiments were not randomized. All quantification and analyses of confocal images were performed blinded. Investigators were not blinded for other experiments. Statistical analyses were performed using Prism 8.0 (Graph Pad Software) and Microsoft Excel. Where appropriate, statistical analyses were performed using an unpaired, two-tailed *t*-test (for comparison of two groups), one-way ANOVA (for comparison of three or more groups), or two-way ANOVA (for grouped analysis). Multiple comparisons analysis was performed using Dunnett's, Tukey's, or Sidak's methods (method was selected based on the recommendation of Prism 8.0 for a given comparison). *P* values less than 0.05 were considered significant. All experiments are represented by multiple biological replicates or independent experiments. The number of replicates per experiment are indicated in the legends. For data presented in Fig. 2h, the data for shControl are representative of 2 independent experiments and the data for shSLC25A51 are representative of 4 independent experiments. More than 30 cells were analysed per condition. For data presented in Extended Data Fig. 1e, the experiment was repeated two independent times; for Extended Data Fig. 1h, NDT1 and vector experiments were repeated 24 times and the experiment for each transporter was repeated 4 times; for Extended Data Fig. 1i the experiment was repeated 4 independent times and more than 20 cells were analysed each time; for Extended Data Fig. 4a, the experiment was repeated 3 times and 9 distinct colonies were tested; for Extended Data Fig. 4b, the experiment was repeated over 10 times with over 10 transformations and 3 colonies were tested for each transformation. This experiment was regularly repeated throughout use of the strain to validate that its growth phenotype was as expected. For Extended Data Fig. 4c, this experiment was repeated over 10 times; including over 10 transformation with 3 colonies tested per transformation. This experiment was regularly repeated throughout use of the strain to validate that no compensatory mutations had been created. For Extended Data Fig. 4d, this experiment was repeated 2 independent times. For Extended Data Fig. 4e, this experiment was performed once with technical triplicates.

Reporting summary

Further information on research design is available in the Nature Research Reporting Summary linked to this paper.

Data availability

The authors declare that the data supporting the findings of this study are available within the paper and its supplementary information files. Source data are provided with this paper.

Code availability

No custom codes were used during this study. Mathematical calculations are described in the materials and methods section or by cited works.

34. Malecki, M. J. et al. Leukemia-associated mutations within the NOTCH1 heterodimerization domain fall into at least two distinct mechanistic classes. *Mol. Cell. Biol.* **26**, 4642–4651 (2006).
35. Eller, J. M. et al. Flow cytometry analysis of free intracellular NAD^+ using a targeted biosensor. *Curr. Protoc. Cytom.* **88**, e54 (2019).
36. Wang, L. et al. Peak annotation and verification engine for untargeted LC–MS metabolomics. *Anal. Chem.* **91**, 1838–1846 (2019).
37. Adusumilli, R. & Mallick, P. Data conversion with ProteoWizard msConvert. *Methods Mol. Biol.* **1550**, 339–368 (2017).
38. Su, X., Lu, W. & Rabinowitz, J. D. Metabolite spectral accuracy on orbitraps. *Anal. Chem.* **89**, 5940–5948 (2017).
39. Chong, J., Wishart, D. S. & Xia, J. Using MetaboAnalyst 4.0 for comprehensive and integrative metabolomics data analysis. *Curr. Protoc. Bioinformatics* **68**, e86 (2019).
40. Amberg, D. C., Burke, D. J. & Strathern, J. N. High-efficiency transformation of yeast. *CSH Protoc* **2006**, pdb.prot4145 (2006).
41. Meisinger, C., Pfanner, N. & Truscott, K. N. Isolation of yeast mitochondria. *Methods Mol. Biol.* **313**, 33–39 (2006).
42. Izawa, T. & Unger, A. K. Isolation of mitochondria from *Saccharomyces cerevisiae*. *Methods Mol. Biol.* **1567**, 33–42 (2017).
43. Bricker, D. K. et al. A mitochondrial pyruvate carrier required for pyruvate uptake in yeast, *Drosophila*, and humans. *Science* **337**, 96–100 (2012).

Acknowledgements We thank all members of the Baur and Cambronne laboratories, V. Moiseenkova-Bell, A. Ellington, E. Marcotte, R. Goodman, I. Heiland, M. Whorton, E. Gouaux and J. Dixon for constructive discussions and suggestions; and M. Blair, Q. Chen, V. Annamalai, X. Yu, A. Slepian and CBRS UT Austin Proteomics Facility for technical support. This work was supported by grants from the National Institutes of Health (R01DK098656 to J.A.B., DP2GM126897 to X.A.C., TL1TR001880, T32AR53461 and F32HL145923 to T.S.L.) and the Norwegian Research Council (250395/F20 to M.Z.).

Author contributions T.S.L., X.A.C. and J.A.B. conceived and designed the overall study. T.S.L., J.M.E., M.-J.L., M.E.M., J.D.R., F.B.J., X.A.C. and J.A.B. contributed to the development of the hypotheses and experimental approaches. T.S.L., J.M.E., M.-J.L., M.N., F.R., M.R.M, C.P., M.R.B. and P.O. performed and analysed experiments. All authors contributed to the interpretation of experiments. T.S.L., X.A.C. and J.A.B. wrote the manuscript. J.M.E., M.-J.L., K.J. and M.Z. edited, and all authors reviewed the manuscript.

Competing interests J.D.R. is a co-founder of Toran Therapeutics. The remaining authors declare no competing interests.

Additional information

Supplementary information is available for this paper at https://doi.org/10.1038/s41586-020-2741-7.

Correspondence and requests for materials should be addressed to X.A.C. or J.A.B.

Peer review information *Nature* thanks Ferdinando Palmieri and the other, anonymous, reviewer(s) for their contribution to the peer review of this work.

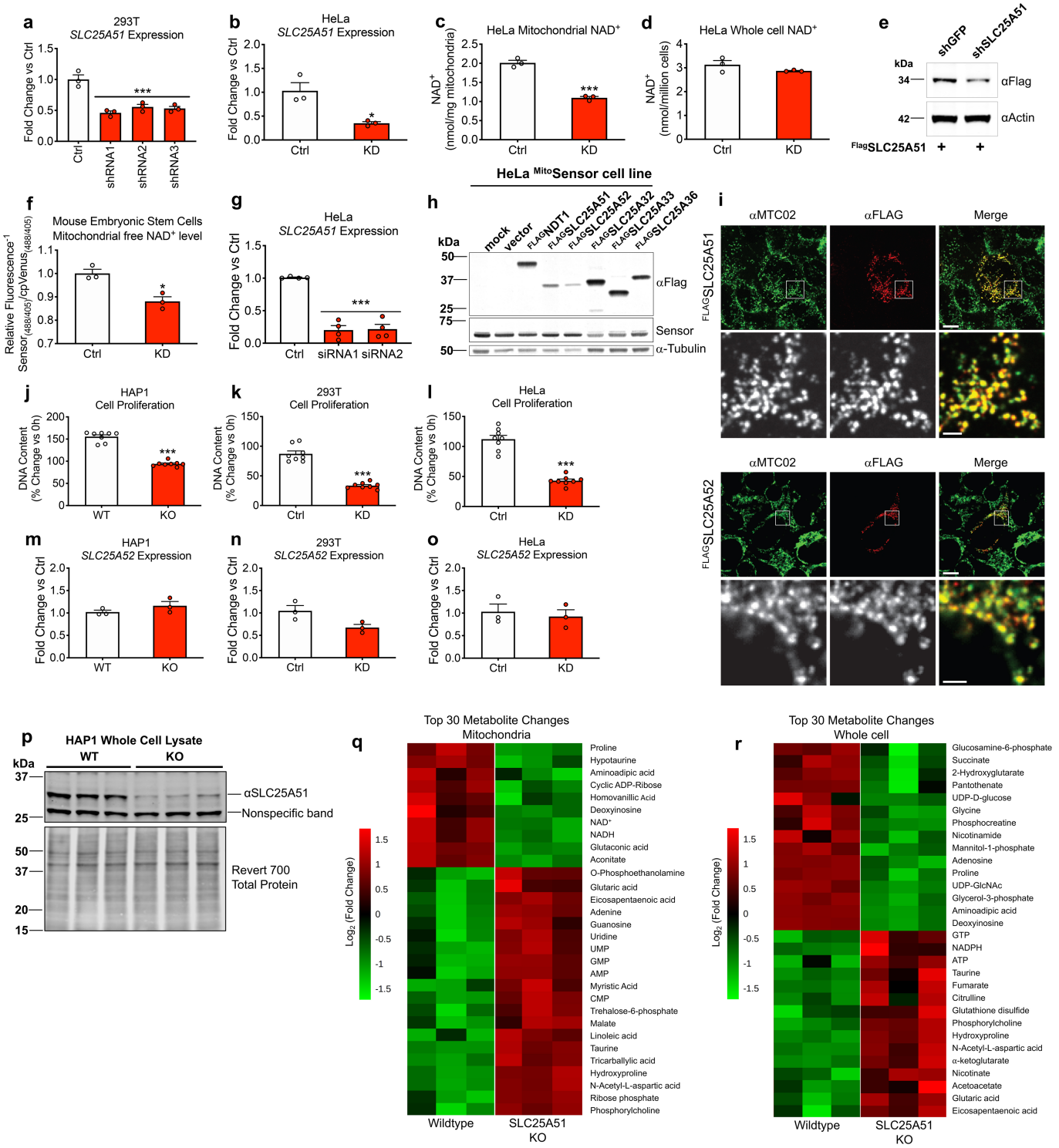

Extended Data Fig. 1 | See next page for caption.

Extended Data Fig. 1 | SLC25A51 is a mitochondrial protein that affects cellular NAD^+ distribution, proliferation, and metabolome profiles. **a**, **b**, qPCR quantification of *SLC25A51* mRNA expression in HEK 293T ($n = 3$) (**a**) and HeLa cells ($n = 3$) (**b**) expressing shRNA targeting *SLC25A51*. **c**, **d**, NAD^+ content of isolated mitochondria ($n = 3$) (**c**) and whole cell lysates ($n = 3$) (**d**) from HeLa cells with stable shRNA knockdown of *SLC25A51* (KD) and non-targeting control (Ctrl). **e**, Western blot confirming shRNA targeting murine *Slc25a51* reduces SLC25A51 protein expression in cells transfected with cDNA encoding SLC25A51-FLAG. **f**, Mitochondrial free NAD^+ levels in mouse embryonic stem cells expressing shRNA against *Slc25a51* and non-targeting shRNA (shFF2), as measured with the mitochondrial cpVenus NAD^+ biosensor ($n = 3$). **g**, qPCR quantification of *SLC25A51* mRNA expression in HeLa cells transfected with siRNA targeting *SLC25A51* ($n = 3$). **h**, Western blot confirming protein expression of Flag-tagged mitochondrial carriers. Controls include stable expression of the NAD^+ biosensor (sensor) and anti-Tubulin for loading. **i**, Immunofluorescent detection of SLC25A51 and SLC25A52 subcellular localization. Cells were transiently transfected with cDNA encoding Flag-HA-tagged SLC25A51 or SLC25A52 and probed with anti-Flag and the mitochondrial marker, anti-MTC02. Scale bar: 10 µM, 2 µM on inset. Inset represents zoomed view of Flag localization and mitochondria. **j**–**l**, Proliferation of HAP1 SLC25A51-KO ($n = 8$) (**j**), HEK 293T *SLC25A51* shRNA-knockdown ($n = 8$) (**k**), HeLa *SLC25A51* shRNA-knockdown cells ($n = 8$) (**l**) and their respective controls. Proliferation was measured by CyQuant, a fluorescent DNA dye, at 0h and 96h after plating and expressed as fold change. **m**–**o**, qPCR quantification of *SLC25A52* mRNA expression in HAP1 SLC25A51-KO (**m**), HEK 293T *SLC25A51* shRNA-knockdown (**n**) and HeLa *SLC25A51* shRNA-knockdown cells ($n = 3$) (**o**). **p**, Western blot of whole cell protein lysates from HAP1 wild type (WT) and SLC25A51 knockout (KO) cells confirming SLC25A51 loss. Loading control is total protein measured by Revert 700 Total Protein. **q**, **r**, Heat map of top 30 mitochondrial (**q**) and whole cell metabolites (**r**) that differ between HAP1 wild type and SLC25A51-KO cells ($n = 3$). Data represented as mean ± SEM. *P* values were determined by unpaired, two-tailed Student's *t*-test (for two groups) or one-way ANOVA with multiple comparisons analysis using Dunnett's method (for groups of three or more). $^*P < 0.05$, and $^{***}P < 0.001$ vs control or WT (exact *P* values are provided in the source data).

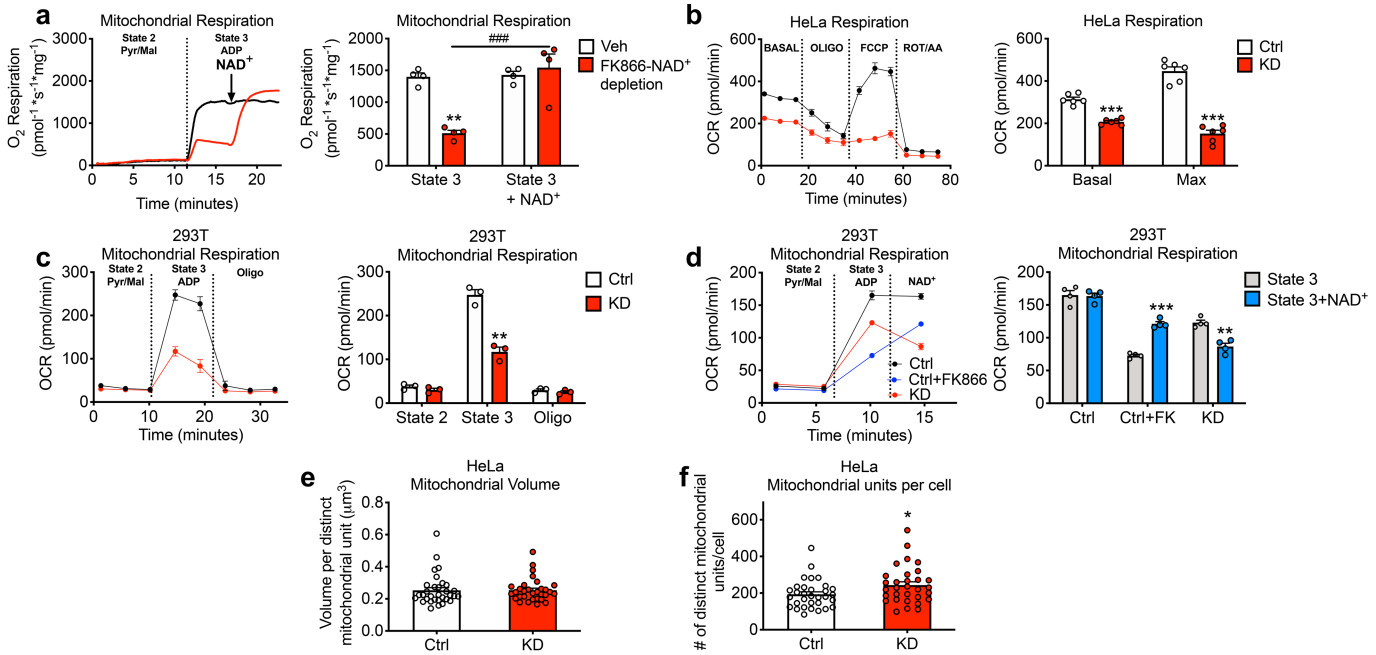

Extended Data Fig. 2 | NAD⁺ and SLC25A51 affect oxidative phosphorylation. a, Respiration of isolated mitochondria from HEK 293T cells treated with either vehicle (Veh) or the NAMPT inhibitor FK866 to deplete mitochondrial NAD⁺. Mitochondria were treated with pyruvate and malate (state 2), then ADP was added to induce state 3 respiration. 1 mM NAD⁺ was added to test the ability of exogenous NAD⁺ to rescue respiration in the setting of mitochondria NAD⁺ depletion (Trace is representative of $n = 4$ independent experiments). *P* values were determined by two-way ANOVA with multiple comparisons analysis using the Sidak method. **b**, Oxygen consumption rate (OCR) was measured in *SLC25A51* shRNA knockdown (KD) and control (Ctrl) HeLa cells using a Seahorse XF96e. Basal OCR was measured before the addition of treatments and maximal respiration was measured after the sequential addition of oligomycin (Oligo, ATP synthase inhibitor) and FCCP (uncoupler). Rotenone (Rot) and Antimycin A (AA) were added as a control to completely block mitochondrial oxygen consumption ($n = 6$). **c**, Respiration of isolated mitochondria from *SLC25A51* knockdown HEK 293T cells. Mitochondria were treated with pyruvate/malate (state 2), and then ADP was added to induce state 3 respiration. Oligomycin was added to block ATP synthase-mediated respiration ($n = 3$ independent experiments). **d**, Mitochondria were isolated from HEK 293T control, *SLC25A51* shRNA knockdown cells, and controls treated with FK866 to deplete mitochondrial NAD⁺. Mitochondrial oxygen consumption rate was measured after treatment with pyruvate/malate (state 2), ADP (state 3), and 1 mM NAD⁺ ($n = 4$ independent experiments). **e**, **f**, Mean volume per mitochondrial unit (**e**) and number of distinct mitochondria per cell (**f**) quantified from confocal image reconstructions of mitochondrial voxels in *SLC25A51* shRNA knockdown ($n = 31$ cells) and control ($n = 32$ cells) HeLa cells. Data represented as mean ± SEM. *P* values were determined by unpaired, two-tailed Student's *t*-test. $^{*}P < 0.05$, $^{**}P < 0.01$, and $^{***}P < 0.001$ vs vehicle or control; $^{###}P < 0.001$ vs state 3 (exact *P* values are provided in the source data).

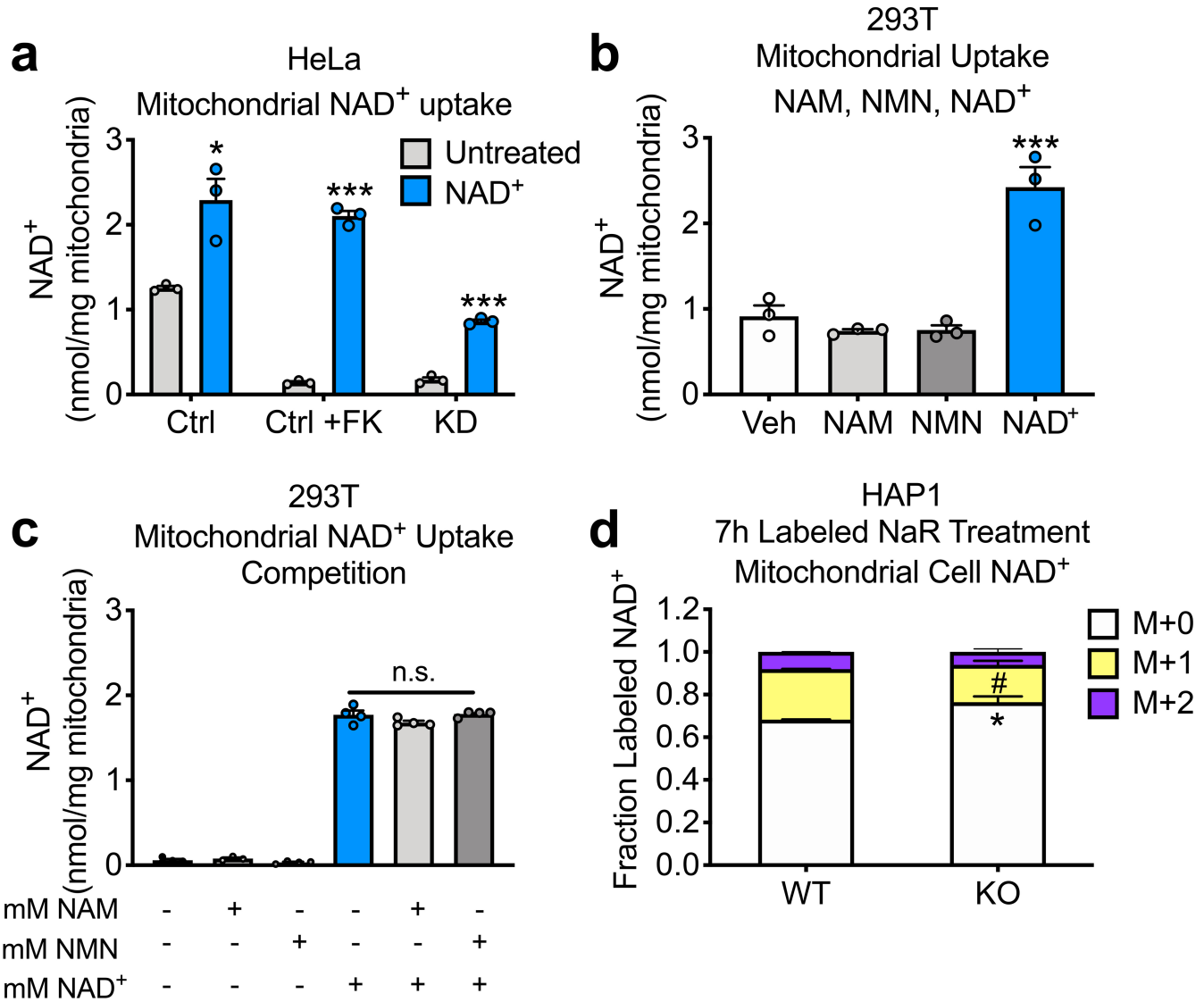

Extended Data Fig. 3 | Intact NAD$^+$, but not nicotinamide or nicotinamide mononucleotide contributes to the mitochondrial NAD$^+$ pool. **a**, Mitochondrial NAD$^+$ content was measured in isolated mitochondria from HeLa control (Ctrl) cells, control cells treated with FK866 (Ctrl+FK), and *SLC25A51* shRNA-knockdown (KD) cells. NAD$^+$ content of isolated mitochondria was determined before (untreated) and after a 40-min incubation with 1 mM NAD$^+$ ($n = 3$ independent experiments). **b**, NAD$^+$ levels in HEK 293T mitochondria incubated with 1 mM nicotinamide (NAM), 1 mM nicotinamide mononucleotide (NMN), or 1 mM NAD$^+$ ($n = 3$ independent experiments). **c**, NAD$^+$ uptake in NAD$^+$-depleted mitochondria isolated from HEK 293T cells incubated with NAD$^+$ ± 2 mM NAM or 2mM NMN ($n = 4$ independent experiments). **d**, Fractional labelling of mitochondrial NAD$^+$ in HAP1 cells treated with isotopically double labelled NaR ($n = 3$ biological independent replicates). Data represented as mean ± SEM. *P* values were determined by unpaired, two-tailed Student's *t*-test (for two groups) or one-way ANOVA with multiple comparisons analysis using Dunnett's or Tukey's method (for groups of three or more). $^*P < 0.05$ and $^{***}P < 0.001$ vs untreated, vehicle, and wild-type M+0; $^{\#}P < 0.05$ vs wild-type M+1.

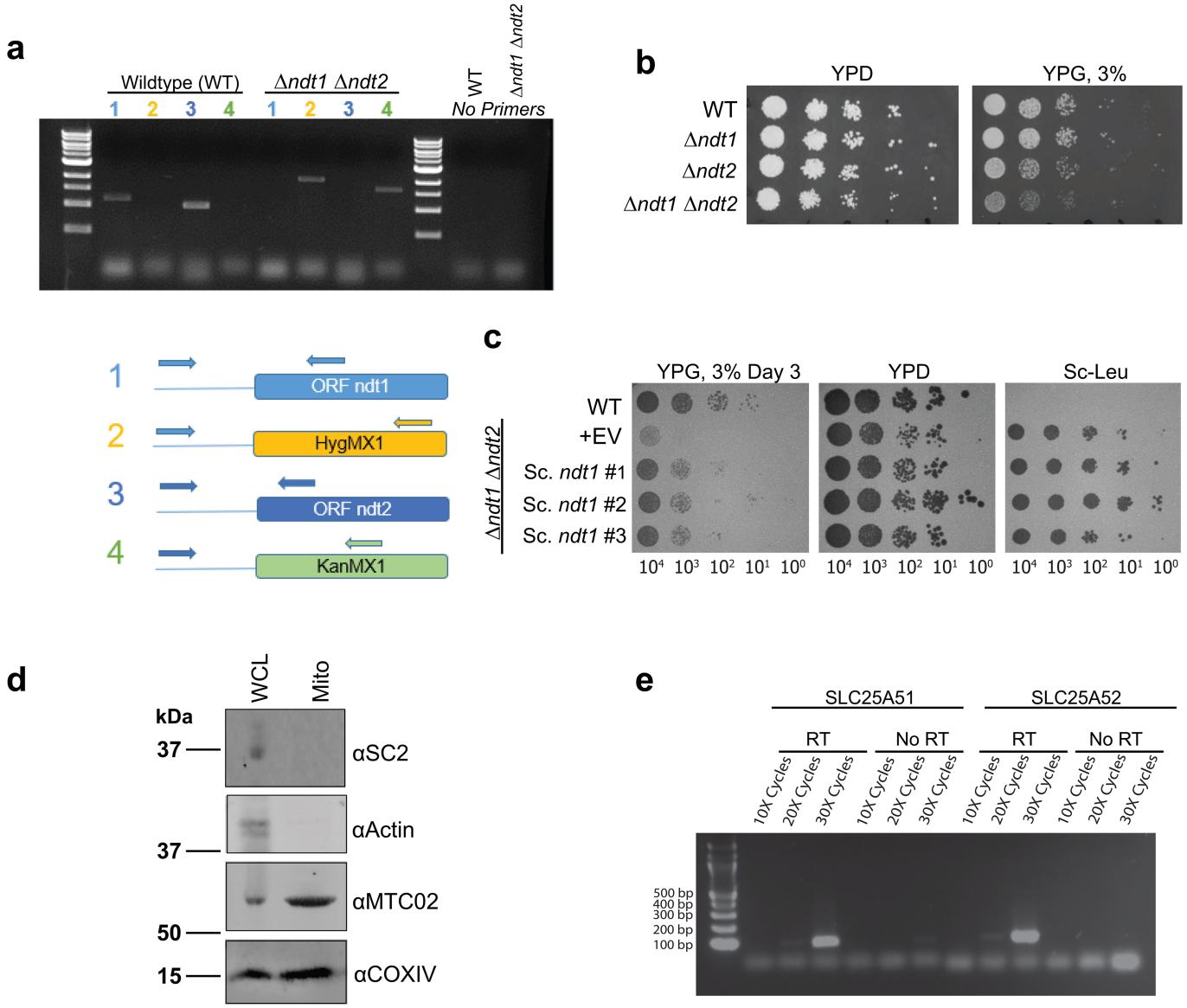

Extended Data Fig. 4 | Generation and validation of yeast strains for testing mitochondrial NAD⁺ transport. a, PCR genotyping to confirm double knockout gene deletion in BY4727 *S. cerevisiae* via antibiotic-resistance cassette replacement at the *NDT1* and *NDT2* loci. **b**, **c**, Deletion of the mitochondrial NAD⁺ carriers *NDT1* and *NDT2* in DKO strain phenocopied previously described growth defects on non-fermentative media (YP, 3% glycerol media)[2], which was rescued by plasmid expression of NDT1. **d**, Western blot confirmed enrichment of mitochondrial markers (MTC02 and COXIV) and absence of cytoplasmic proteins (actin) or ER (SC2) in isolated mitochondria from yeast. **e**, RT-PCR confirmed ectopic expression from pRS415-*SLC25A51* and pRS415-*SLC25A52* in DKO strains.

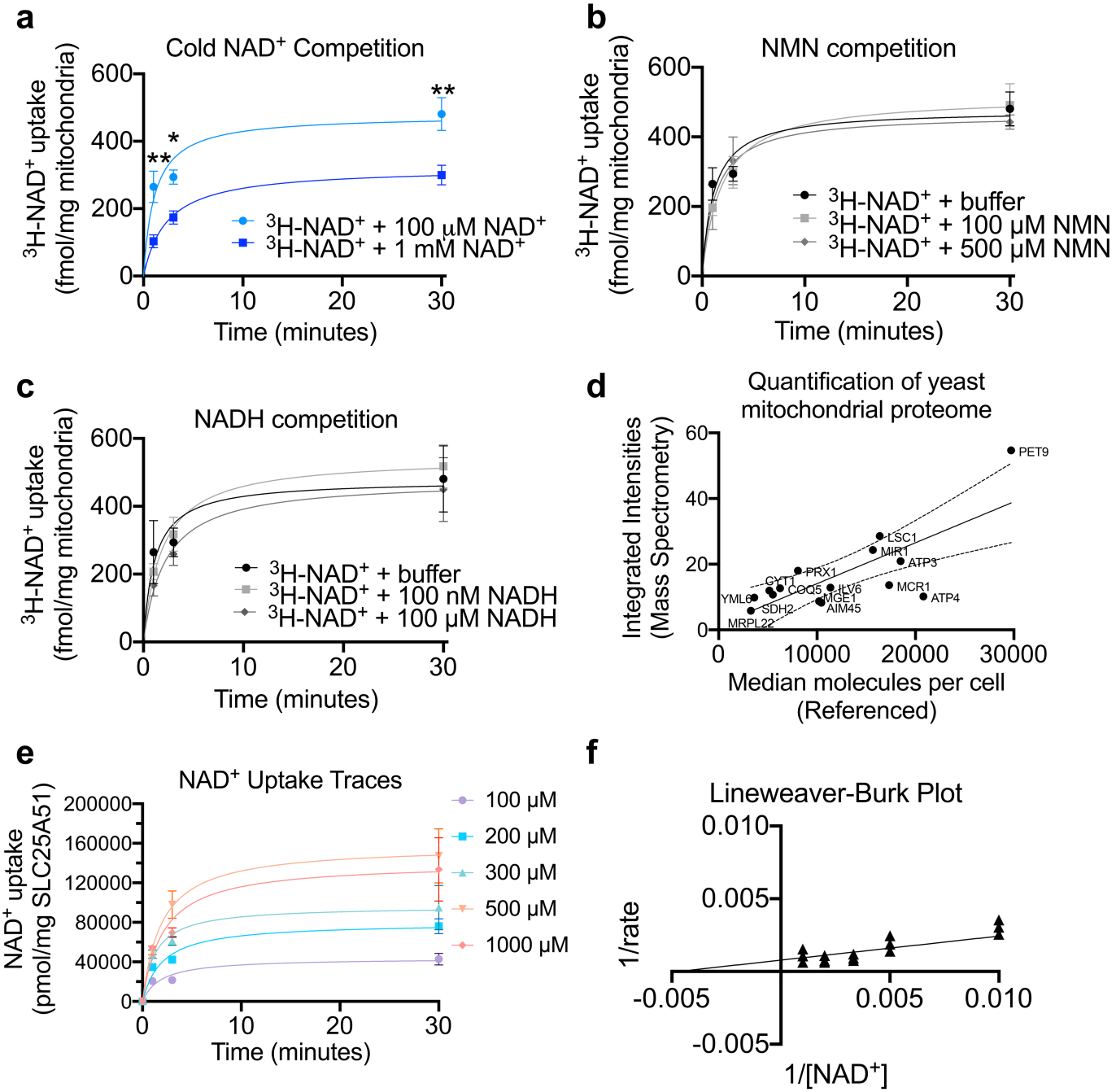

Extended Data Fig. 5 | Kinetics and selectivity of NAD⁺ transport by human SLC25A51 expressed in yeast mitochondria. a–**c**,, Co-incubation with excess unlabelled NAD⁺ ($n = 5$ independent experiments for 1 mM NAD⁺) (**a**), supraphysiological levels of NMN (100 µM, $n = 4$ independent experiments; 500 µM, $n = 5$ independent experiments) (**b**), NADH ($n = 3$ independent experiments) with ^{3}H-NAD⁺ to measure uptake competition in mitochondria from DKO yeast expressing SLC25A51 (**c**). **d**, Proportional relationship between integrated peak intensities from mass spectrometry of mitochondrial samples compared to a known meta data set of absolute protein abundances; used to quantitate SLC25A51 abundance in yeast samples. **e**, Uptake measured with indicated NAD⁺ concentrations; calculated from specific activity ($n = 3$ independent experiments, mean ± SEM). **f**, Lineweaver-Burk plot based on a nonlinear fit with datapoints overlaid ($n = 3$ independent experiments). *P* values were determined by two-way ANOVA with multiple comparisons analysis using Sidak's method. $^*P < 0.05$ and $^{**}P < 0.01$ vs 100 µM cold NAD⁺.

Extended Data Table 1 | Essential mitochondrial solute carrier family 25 genes determined by genome-wide CRISPR/Cas9 screens examining cellular viability

Essential *SLC25A* Genes	Cell lines where gene is essential/ Cell lines tested	Citation	Annotation	Distribution of Expression in Tissues
SLC25A1	(2/4) (1/1)	Wang *et al.* Science, 2015 Bertomeu *et al.* MCB, 2017	Mitochondrial Tricarboxylate Transport Protein	All tissues
SLC25A3	(1/4) (1/1) (2/2) (2/5)	Wang *et al.* Science, 2015 Bertomeu *et al.* MCB, 2017 Blomen *et al.* Science, 2015 Hart *et al.* Cell, 2015	Mitochondrial Phosphate Carrier Protein	All tissues; Enriched in Heart and Skeletal Muscle
SLC25A5	(1/2)	Blomen *et al.* Science, 2015	ADP/ATP translocase 2	All tissues
SLC25A10	(5/5)	Hart *et al.* Cell, 2015	Mitochondrial Dicarboxylate Carrier	All tissues; Enriched in liver
SLC25A14	(1/4)	Wang *et al.* Science, 2015	Mitochondrial Uncoupling Protein 5	All tissues
SLC25A19	(1/1) (2/2) (2/5)	Bertomeu *et al.* MCB, 2017 Blomen *et al.* Science, 2015 Hart *et al.* Cell, 2015	Mitochondrial Thiamine Pyrophosphate Carrier	All tissues; Enriched in testis
SLC25A22	(2/5)	Hart *et al.* Cell, 2015	Mitochondrial Glutamate Carrier 1	All tissues; Enriched in brain and pancreas
SLC25A25	(1/5)	Hart *et al.* Cell, 2015	Calcium-binding Mitochondrial Carrier Protein SCaMC-2	All tissues
SLC25A26	(1/4) (1/1) (2/2) (3/5)	Wang *et al.* Science, 2015 Bertomeu *et al.* MCB, 2017 Blomen *et al.* Science, 2015 Hart *et al.* Cell, 2015	Mitochondrial S-Adenosylmethionine Carrier Protein	All tissues
SLC25A28	(4/5)	Hart *et al.* Cell, 2015	Mitoferrin-2	All tissues
SLC25A29	(1/5)	Hart *et al.* Cell, 2015	Mitochondrial Basic Amino Acids Transporter	All tissues; Enhanced in thyroid gland
SLC25A31	(1/5)	Hart *et al.* Cell, 2015	ADP/ATP translocase 4	Enriched in testis
SLC25A32	(1/4)	Wang *et al.* Science, 2015	Mitochondrial Folate Carrier	All tissues
SLC25A39	(1/5)	Hart *et al.* Cell, 2015	Unannotated; Heme biosynthetic process and transmembrane transport	All tissues
SLC25A41	(1/5)	Hart *et al.* Cell, 2015	Unannotated; ATP transmembrane transporter activity	Detected in some; Enriched in brain and testis
SLC25A42	(2/5)	Hart *et al.* Cell, 2015	Mitochondrial Coenzyme A Transporter	All tissues; Enriched in liver
SLC25A43	(1/4)	Wang *et al.* Science 2015	Unannotated; ATP transmembrane transporter activity	All tissues
SLC25A45	(1/4) (3/5)	Wang *et al.* Science, 2015 Hart *et al.* Cell, 2015	Unannotated; Acyl carnitine transmembrane and ATP transmembrane transporter activity	All tissues; Enriched in pancreas
SLC25A51[#]	(3/4) (1/1)	Wang *et al.* Science, 2015 Bertomeu *et al.* MCB, 2017	Unannotated; No prediction	All tissues

Table includes essential gene name, number of cell lines in which gene is essential, number of cell lines tested, corresponding citation of study using genome-wide CRISPR/Cas9 screens to determine essential genes, annotation (Uniprot), and tissue expression profile (Human Protein Atlas[20]). [#]*SLC25A51* was not tested in Hart et al. refs. [6,7,22,23].

Extended Data Table 2 | Initial NAD^+ uptake rates calculated from specific activity in isolated mitochondria

	n	*Initial Rates (pmol/min/mg mitochondria)*	*Std deviation*	*P value vs WT*	*P value vs DKO*	*P value vs A51*
Wildtype	4	7.6	± 1.5			
DKO	4	-0.08	± 1.8	0.0006		
DKO + SLC25A51	4	12.1	± 2.8	0.0315	0.0003	
DKO + SLC25A52	3	4.3	± 1.5	0.0385	0.0180	0.0082
DKO + SLC25A51 + 100 nM NADH	3	14	± 3.4	0.0196	0.0008	0.4660
DKO + SLC25A51 + 100 µM NADH	3	10	± 2.3	0.1504	0.0011	0.3434
DKO + SLC25A51 + 100 µM NMN	4	12.7	± 6.2	0.8193	0.0040	0.0474
DKO + SLC25A51 + 500 µM NMN	5	15	± 10.4	0.2114	0.0261	0.6212

P values were determined by unpaired, two-tailed Student's *t*-test.

nature research

Corresponding author(s): Xiaolu A. Cambronne and Joseph A. Baur

Last updated by author(s): Aug 23, 2020

Reporting Summary

Nature Research wishes to improve the reproducibility of the work that we publish. This form provides structure for consistency and transparency in reporting. For further information on Nature Research policies, see our Editorial Policies and the Editorial Policy Checklist.

Statistics

For all statistical analyses, confirm that the following items are present in the figure legend, table legend, main text, or Methods section.

n/a	Confirmed	
☐	☒	The exact sample size (*n*) for each experimental group/condition, given as a discrete number and unit of measurement
☐	☒	A statement on whether measurements were taken from distinct samples or whether the same sample was measured repeatedly
☐	☒	The statistical test(s) used AND whether they are one- or two-sided *Only common tests should be described solely by name; describe more complex techniques in the Methods section.*
☐	☒	A description of all covariates tested
☐	☒	A description of any assumptions or corrections, such as tests of normality and adjustment for multiple comparisons
☐	☒	A full description of the statistical parameters including central tendency (e.g. means) or other basic estimates (e.g. regression coefficient) AND variation (e.g. standard deviation) or associated estimates of uncertainty (e.g. confidence intervals)
☐	☒	For null hypothesis testing, the test statistic (e.g. *F*, *t*, *r*) with confidence intervals, effect sizes, degrees of freedom and *P* value noted *Give P values as exact values whenever suitable.*
☒	☐	For Bayesian analysis, information on the choice of priors and Markov chain Monte Carlo settings
☒	☐	For hierarchical and complex designs, identification of the appropriate level for tests and full reporting of outcomes
☒	☐	Estimates of effect sizes (e.g. Cohen's *d*, Pearson's *r*), indicating how they were calculated

Our web collection on statistics for biologists contains articles on many of the points above.

Software and code

Policy information about availability of computer code

Data collection	Acea NovoExpress 1.3.0, Olympus CellSens Dimensions 2.3
Data analysis	Graphpad Prism 8.2, BD FlowJo 10.5.3, Bitplane Imaris x64 8.4.1, MAVEN 3.1, MetaboAnalyst 3.0, and AccuCor algorithm described in Su, Lu and Rabinowitz, 2017, doi:10.1021/acs.analchem.7b00396.

For manuscripts utilizing custom algorithms or software that are central to the research but not yet described in published literature, software must be made available to editors and reviewers. We strongly encourage code deposition in a community repository (e.g. GitHub). See the Nature Research guidelines for submitting code & software for further information.

Data

Policy information about availability of data

All manuscripts must include a data availability statement. This statement should provide the following information, where applicable:

- Accession codes, unique identifiers, or web links for publicly available datasets
- A list of figures that have associated raw data
- A description of any restrictions on data availability

The authors declare that the data supporting the findings of this study are available within the paper and its supplementary information files.

Field-specific reporting

Please select the one below that is the best fit for your research. If you are not sure, read the appropriate sections before making your selection.

☒ Life sciences ☐ Behavioural & social sciences ☐ Ecological, evolutionary & environmental sciences

For a reference copy of the document with all sections, see nature.com/documents/nr-reporting-summary-flat.pdf

Life sciences study design

All studies must disclose on these points even when the disclosure is negative.

Sample size	Sample size for flow cytometry data collection was set based on analyzing 10 000 fluorescent single cells. Power analyses with alpha 0.05, beta 0.8, was used to determine the minimum number cells to analyze for HeLa mitochondrial morphology. Sample sizes for all other experiments were empirically determined or defined by instrumentation parameters.
Data exclusions	Any indicated data points not included in a time-series was because of technical error or loss of sample. For kinetic estimates, 3 independent series of NAD+ concentrations were used; extra data points that were not encompassed by a full concentration series were not included in the kinetic calculations.
Replication	All experiments are represented by multiple biological replicates, as indicated in the legends and the Statistics and Reproducibility section in Methods. All experiments used low passaged cell lines, and data was collected within 5 passages of transduction for all experiments wherein SLC25A51 was stably depleted or deleted.
Randomization	Samples were classified within experimental groups based on their treatment only. To the extent possible, the indicated treatment was the only variable considered when performing comparisons.
Blinding	Any quantitations using non-instrumental measurements were blinded. E.g. the imaging and analyses of HeLa mitochondrial volumes was performed blinded.

Reporting for specific materials, systems and methods

We require information from authors about some types of materials, experimental systems and methods used in many studies. Here, indicate whether each material, system or method listed is relevant to your study. If you are not sure if a list item applies to your research, read the appropriate section before selecting a response.

Materials & experimental systems

n/a	Involved in the study
☐	☒ Antibodies
☐	☒ Eukaryotic cell lines
☒	☐ Palaeontology and archaeology
☒	☐ Animals and other organisms
☒	☐ Human research participants
☒	☐ Clinical data
☒	☐ Dual use research of concern

Methods

n/a	Involved in the study
☒	☐ ChIP-seq
☐	☒ Flow cytometry
☒	☐ MRI-based neuroimaging

Antibodies

Antibodies used	anti-SLC25A51 (ProSci: #55-424, 1:200), anti-Flag M2 (Sigma: #F1804, 1:3000), anti-α-Tubulin (Sigma #T9026, 1:3000), anti-Total OXPHOS (Abcam: #ab110413, 1:2000), anti-TOM20 (Santa Cruz Biotechnology: # sc-17764), anti-PAR 10H (Enzo: # LX-804-220-R100; 1:6,000), anti-GFP JL-8 (Takara Clontech: #632381); 1:15,000), anti-SC2 (Novus Bio #NBP1-92465, 1:1000), anti-Actin (Abcam #ab14128, 1:1000), anti-MTC02 (Abcam #ab9479, 1:1000 for WB or 1:200 for IF), anti-CoxIV (Abcam #ab33985, 1:1000), β-tubulin (Sigma: #T5293, 1:10,000) and anti-mouse IgG H&L IRDye® 800CW (Abcam #ab216772, 1: 10,000), IRDye® 680RD Goat anti-Mouse IgG (LiCOR: # 926-68070, 1:12,000), IRDye® 800CW Donkey anti-Rabbit IgG (LiCOR: # 926-32213, 1:12,000), Goat anti-Mouse IgG - Alexa Fluor 488 (Invitrogen A-11001, 1:1000); Goat anti-Rabbit IgG - Alexa Fluor 568 (Invitrogen A-11036, 1:1000).
Validation	All antibodies used in this study were commercially developed. With multiple commercial options for each antibody, we selected those that had validating statements in their datasheets, multiple published references, and clear instructions and tested concentrations for its use for our intended purposes. To confirm that we were detecting the protein of interest in our experiments, we confirmed that the detected band migrated to the expected size, and where possible we confirmed loss of that specific band with gene-specific KO or RNAi depletions, as well as its co-migration with product from its ORF cDNA expressed from a plasmid. Only antibodies that specifically detected the protein of interest from a whole cell lysate Western Blot were used for immunofluorescence (IF). Primary antibody specificity for IF was similarly determined by looking for loss or enhancement of signal with gene-specific RNAi or ORF ectopic expression, respectively. Controls without any primary antibody was used to control for non-specific secondary antibody effects.

Eukaryotic cell lines

Policy information about cell lines

Cell line source(s)	HEK293T (ATCC: CRL-3216), HEK293 (ATCC: CRL-1573), HeLa (ATCC: CCL-2), U2OS (ECACC #92022711), HAP1 wildtype (Horizon Discovery: C631), HAP1 SLC25A51 knockout (Horizon Discovery: HZGHC001927c010), J1 murine embryonic stem cells (ATCC: SCRC-1010)
Authentication	Cells were authenticated by the source and checked in lab for appropriate morphology. In the case of J1 mESCs, we routinely assessed their ability to differentiate, as well as retention of positive Alkaline Phosphatase staining.
Mycoplasma contamination	All cell lines were tested routinely for mycoplasma contamination either by PCR analysis or the Lonza MycoAlert mycoplasma detection kit. If mycoplasma was detected, the cell line was discarded and any results acquired from the contaminated cell lines were reconfirmed in mycoplasma negative cells.
Commonly misidentified lines (See ICLAC register)	None were used.

Flow Cytometry

Plots

Confirm that:

☒ The axis labels state the marker and fluorochrome used (e.g. CD4-FITC).

☒ The axis scales are clearly visible. Include numbers along axes only for bottom left plot of group (a 'group' is an analysis of identical markers).

☒ All plots are contour plots with outliers or pseudocolor plots.

☒ A numerical value for number of cells or percentage (with statistics) is provided.

Methodology

Sample preparation	Analyses were performed on live dissociated single type cells.
Instrument	BD LSRII, BD FACS Melody, NovoCyte flow cytometer
Software	FlowJo 10.5.3
Cell population abundance	A minimum of 10 000 fluorescent cells were analyzed for each fluorescent measurement.
Gating strategy	Cells were identified with FCS/SSC gates, debris and doublets were excluded, and fluorescent cells were identified based on non-fluorescent cell controls.

☒ Tick this box to confirm that a figure exemplifying the gating strategy is provided in the Supplementary Information.